Check for updates

Received: 9 December 2025 | Revised: 17 April 2026 | Accepted: 9 May 2026

DOI: 10.1002/alz.71572

Alzheimer's & Dementia®
THE JOURNAL OF THE ALZHEIMER'S ASSOCIATION

RESEARCH ARTICLE

Elimination of tau tangles and soluble aggregates with the small molecule ACI-16664 prevents neurodegeneration in vivo

Nicolas Preitner | Véronique Dehlinger | Patrick Rodriguez | Kerstin Fabbri | Yvan Varisco | Matteo Pigni | Alessandra Lovison | Lucas Münzenmaier | Kasia Piorkowska | Aline Fuchs | Nadine Ait-Bouziad | Nicolas Fournier | Sandra Jepaul | Jérôme Molette | Emanuele Gabellieri | Vincent Darmency | Sonia Poli | Andrea Pfeifer | Marie Kosco-Vilbois | Francesca Capotosti

AC Immune SA, Lausanne, Switzerland

Correspondence
Nicolas Preitner and Francesca Capotosti, AC Immune SA; Lausanne, Switzerland.
Email: nicolas.preitner@acimmune.com and francesca.capotosti@acimmune.com

Funding information
AC Immune SA

Abstract

INTRODUCTION: Pathological tau aggregates are key therapeutic targets in Alzheimer's disease (AD), but current approaches face limitations including poor intracellular penetration, lack of selectivity for aggregated over physiological tau, or reliance on invasive administration.

METHODS: ACI-16664, an orally available brain penetrant tau aggregation inhibitor, was identified through medicinal chemistry optimization of the Morphomer library and characterized using biochemical assays, neuronal cultures, and the Tg4510 tauopathy mouse model.

RESULTS: ACI-16664 selectively bound aggregated tau with high apparent affinity, destabilized its β-sheet structures, blocked intracellular seeding by both soluble and insoluble tau, and prevented tau-induced neurotoxicity. In Tg4510 mice, ACI-16664 reduced both soluble tau aggregates and tangles, and prevented neuronal loss, synaptic degeneration, and cortical atrophy.

DISCUSSION: These findings demonstrate the therapeutic value of targeting tau aggregation across its diverse pathological forms and cellular compartments, supporting the potential of this approach to benefit patients with AD and other tauopathies across disease stages.

KEYWORDS
Alzheimer's disease, cortical atrophy, neurodegeneration, neurofibrillary tangles, small molecule, soluble high-molecular-weight tau, soluble tau aggregates, synapses, tau aggregation inhibitor, tau oligomers, tau pathology, tau seeding, tauopathy

Highlights

- ACI-16664 is an orally available, CNS-penetrant small-molecule inhibitor of tau aggregation.

This is an open access article under the terms of the Creative Commons Attribution-NonCommercial-NoDerivs License, which permits use and distribution in any medium, provided the original work is properly cited, the use is non-commercial and no modifications or adaptations are made.
© 2026 AC Immune SA. *Alzheimer's & Dementia* published by Wiley Periodicals LLC on behalf of Alzheimer's Association.

- Selectively binds and destabilizes pathological β sheets in tau aggregates
- Blocks seeding induced by both soluble and insoluble tau species in neurons
- Prevents neuronal and synaptic loss and cortical atrophy in Tg4510 tauopathy mice

1 | BACKGROUND

Tauopathies, including Alzheimer's disease (AD), frontotemporal dementia (FTD), and progressive supranuclear palsy (PSP), are progressive neurodegenerative disorders characterized by misfolding and aggregation of tau. Tau is a microtubule-associated protein that stabilizes microtubules in neurons and plays key roles in axonal transport, synaptic signaling and plasticity, mitochondrial regulation, DNA protection, and transcription.[1] However, in tauopathies, tau forms toxic aggregates that impair neuronal function and promote neurodegeneration. Tau aggregation is strongly associated with cognitive decline in humans and thought to be a key driver of neurodegeneration.[2,3] Pathogenic point mutations in the MAPT gene in humans cause autosomal dominant forms of FTD with robust tau aggregation, providing genetic evidence that tau pathology can drive neurodegeneration. Moreover, in AD, while tau aggregation is not driven by MAPT mutations, tau pathology correlates closely with cognitive decline, more strongly than amyloid beta (Aβ) plaques.[4–7] Consequently, tau has emerged as a key therapeutic target. To date, however, development of effective therapies has been challenged by the diversity of pathological tau species including insoluble and soluble aggregates.[8,9]

Insoluble tau aggregates mostly accumulate intracellularly within neurons and consist of misfolded tau polymerized into filaments that further assemble into larger structures, such as neurofibrillary tangles (NFTs) in AD. Clinically, NFT abundance and distribution are used to stage AD progression by neuropathological evaluation at autopsy and more recently using tau positron emission tomography (PET) imaging.[10] Longitudinal studies associating tau burden with cognition and neurodegeneration have led to the hypothesis that NFT accumulation precedes neurodegeneration. Interestingly, however, the presence of NFTs does not always result in neuronal death, and, conversely, neuronal and synaptic loss often occur in their absence,[11–13] suggesting other forms of tau contribute to toxicity and disease progression.

Recent studies support the idea that soluble tau aggregates, for example, oligomers and short fibrils, are key drivers of disease progression. Soluble aggregates exist intra- and extracellularly and abnormally accumulate at synapses in AD patients.[14,15] These species propagate between neurons, acting as seeds that induce further misfolding and aggregation of tau. This prion-like spreading process is thought to underlie the progressive nature of AD and other tauopathies, as pathology moves between interconnected brain regions.[16–19] Additionally, tau oligomers at synapses are linked to synaptic engulfment by microglia and astrocytes in AD patients, consistent with a toxic function.[20] Supporting this, animal studies show that soluble tau aggregates disrupt synaptic function and cause cognitive deficits.[21–23] Together, these studies highlight the importance of multiple soluble tau species, particularly small oligomers recognized by the anti-tau antibody T22[24] and larger soluble high-molecular-weight (HMW) tau aggregates.[17,23,25] Both species are detected in AD patients, have been shown experimentally to mediate spreading and toxicity, and are proposed therapeutic targets.

Tau-targeted therapies show promise in animal models, reducing tau pathology.[8] However, available datasets remain limited by important caveats such as targeting only a limited subset of pathological tau species, being confined to the extracellular space, or lacking selectivity for the pathological forms of tau. These limitations likely underlie the modest benefits observed to date in clinical trials.[8,9] Moreover, while targeting extracellular tau species may offer benefits at earlier stages when propagation is thought to be a key driver of disease progression, targeting intracellular aggregation will likely be essential for maximal efficacy at more advanced stages.[16,26,27]

Here, we describe the in vitro and in vivo effects of ACI-16664, a novel orally available, brain-penetrant small molecule acting in both extra- and intracellular compartments to target soluble and insoluble pathological tau. ACI-16664 disrupts pre-formed pathological tau β sheets and, in a tauopathy mouse model, extensively reduced tau pathology, preventing neurodegeneration. These findings highlight a powerful approach for specifically targeting tau-mediated pathology. ACI-16664's comprehensive mechanism of action against pathological tau aggregates demonstrates that small molecules capable of remodeling tau fibrils may represent a unique therapeutic opportunity to counteract pre-existing tau pathology and hinder its progression in AD and other tauopathies.

2 | MATERIALS AND METHODS

2.1 | Isolation and characterization of tau paired helical filaments (PHFs)

Fresh-frozen *post mortem* brain samples from AD donors (Braak stages V–VI; neocortical regions, predominantly frontal cortex) were obtained from Banner Health, Tissue Solutions, and the Netherlands Brain Bank. Tau pathology was confirmed by Thioflavin S (ThioS) (Santa Cruz) staining and immunohistochemistry (IHC) using the AT8 monoclonal antibody (MN1020, Thermo Fisher Scientific) to confirm the presence of tau pathology. PHFs were isolated following a protocol adapted from Rostagno et al.[28] Brain samples were thawed on ice, and visible white matter, meninges, and large blood vessels were removed. Gray matter was dissected and homogenized in ice-cold homogenization buffer (0.75 M NaCl, 100 mM MES, 1 mM EGTA, 0.5 mM $MgSO_4$, 2 mM DTT, protease inhibitor cocktail [Roche, Catalog No.:04693124001], 1 tablet/50 mL) at a ratio of 3 mL per gram of tissue. The homogenate was incubated on ice for 20 min and centrifuged at 11,000 × g for 20 min at 4°C. The supernatant was then centrifuged at 100,000 × g for 60 min at 4°C. The supernatant (S7a) was snap-frozen in liquid nitrogen and stored at −80°C for the

15525279, 2026, 7, Downloaded from https://alz-journals.onlinelibrary.wiley.com/doi/10.1002/alz.71572 by Schweizerische Akademie Der, Wiley Online Library on [03/07/2026]. See the Terms and Conditions (https://onlinelibrary.wiley.com/terms-and-conditions) on Wiley Online Library for rules of use; OA articles are governed by the applicable Creative Commons License

RESEARCH IN CONTEXT

1. **Systematic review:** We reviewed therapeutic strategies targeting tauopathies using PubMed and conference sources. Although no disease-modifying tau-directed therapies are approved, several approaches – antisense oligonucleotides, siRNAs, active and passive immunotherapies, and small molecules – are under evaluation. Early clinical findings are encouraging; however, most approaches face limitations such as invasive delivery, poor selectivity for pathological tau, low CNS penetration, or lack of intracellular activity.
2. **Interpretation:** ACI-16664 is an orally available, brain-penetrant small molecule. In vitro, it eliminates pathological tau beta sheets, inhibits aggregation, and blocks tau seeding and toxicity. In vivo, ACI-16664 broadly reduces pathological tau species, including soluble HMW aggregates and neurofibrillary tangles, and prevents neuronal loss, synaptic degeneration, and cortical atrophy. The mode of action of ACI-16664 is expected to translate into meaningful clinical benefits for individuals with tauopathies, including AD.
3. **Future directions:** Ongoing studies aim to further characterize ACI-16664 and, if needed, optimize its developability profile to support advancement toward clinical evaluation.

isolation of soluble HMW tau aggregates. Pellets from both centrifugation steps were resuspended in extraction buffer (10 mM Tris-HCl, 10% sucrose, 0.85 M NaCl, 1 mM EGTA, protease inhibitor cocktail [Roche, Catalog No.: 04693124001], and phosphatase inhibitor cocktails 2 and 3 [Sigma-Aldrich, Catalog No.: P5726 and Catalog No.: P0044]) in a final volume of 10 mL per gram of gray matter. The resuspended material was centrifuged at 15,000 × g for 20 min at 4°C. The resulting supernatant was mixed by inversion at room temperature for 60 min in the presence of 1% Sarkosyl and then centrifuged at 100,000 × g for 60 min at 4°C. The PHF-containing pellet was washed extensively with phosphate-buffered saline (PBS) to remove residual Sarkosyl and resuspended in 50 µL of PBS per gram of starting gray matter by pipetting and sonication. Each PHF batch was characterized using AlphaLISA assays: Total tau was quantified with the Tau13/HT7 antibody pair, phosphorylated tau at Ser202/Thr205 with AT8/HT7, and aggregated tau with HT7/HT7. In the seeding assay and neuronal toxicity experiments, pools of PHFs were used to account for individual patient differences. Each pool was prepared by mixing individual preparations from at least six AD donors. Experiments were repeated with several pools of AD donors.

2.2 | Isolation of insoluble Aβ

Fresh-frozen *post mortem* brain samples from AD donors with confirmed burden of tau and Aβ aggregates were homogenized in three volumes (1:3, w/v) of high salt buffer (50 mM Tris-HCl pH 7.5, 750 mM NaCl, 5 mM EDTA) supplemented with protease inhibitors (Complete; Roche, Catalog No.:11697498001) at 4°C with a glass Dounce homogenizer. The homogenate was transferred to polycarbonate centrifuge bottles (16 × 76 mm; Beckman Catalog No.: 355603) and centrifuged at 100,000 x g (38,000 rpm) in an ultracentrifuge (Beckman, XL100K) for 60 min at 4°C using the pre-cooled 70.1 rotor (Beckman, Catalog No.: 342184). Pellets were resuspended in high salt buffer supplemented with 1% Triton X-100 and homogenized at 4°C with a syringe. The homogenates were centrifuged again at 100,000 x g (38,000 RPM, 70.1 rotor) for 60 min at 4°C. Pellets were resuspended in high salt buffer supplemented with 1% Triton X-100 and 1 M sucrose and homogenized at 4°C with a syringe. The homogenates were centrifuged at 100,000 x g (38,000 rpm, 70.1 rotor) for 60 min at 4°C. The resulting pellets containing insoluble fraction (IF) were resuspended in 1.5 mL PBS per gram of starting material, aliquoted, and stored at −80°C until use.

2.3 | Isolation of soluble HMW tau aggregates from AD brain

To enrich for AD-derived HMW soluble tau aggregates, the S7a fractions (described above) from five AD donors were pooled, filtered using a syringe filter (Millex-GV Syringe Filter Unit, 0.22 µm, PVDF, 33 mm), fractionated through size exclusion chromatography (SEC) using an analytical Superose 6 Increase 10/300 GL column (Cytiva), and eluted in PBS. Protein elution profiles were monitored by ultraviolet absorbance at 214 nm. All the elution fractions (1 mL each) were collected. Fractions were analyzed by AlphaLISA for aggregated tau using the HT7/HT7 antibody couple (Invitrogen, Catalog No.: MN1000B / Invitrogen, Catalog No.: MN1000) and aggregate-rich fractions (Fraction 6 and 7), which contained the AD-derived soluble HMW tau aggregates, were pooled.

2.4 | Thioflavin T (ThT)-based fluorescence assay

To assess compound activity on pre-formed recombinant tau aggregates, full-length human tau (hTau) (2N4R; 441 amino acids), obtained by expression in bacteria and subsequent purification (Boston Biochem), was aggregated using either heparin or tau PHFs as seeds. For heparin-induced aggregation, recombinant 2N4R tau at 35 µM in PBS was mixed with 25 µM of heparin (Sigma-Aldrich) and 10 mM of DTT (Sigma-Aldrich) and incubated in a Thermomixer (Eppendorf) for 72 h at 37°C with shaking at 1000 rpm. For PHF-seeded aggregation, recombinant 2N4R tau at 35 µM was mixed with human AD brain-derived PHF at a final dilution of 1:800 and incubated in a Thermomixer for 72 h at 37°C with shaking at 1000 rpm. Recombinant Aβ1-42 peptide film (Bachem, Catalog No.: 4014447) at 48 mM was thawed for 10 min at room temperature (RT), diluted in DMSO to 5 mM, sonicated in a water bath for 30 s, diluted in PBS to 75 µM, and aggregated in a Thermomixer for 4 days at 37°C with shaking at 300 rpm.

15525279, 2026, 7, Downloaded from https://alz-journals.onlinelibrary.wiley.com/doi/10.1002/alz.71572 by Schweizerische Akademie Der, Wiley Online Library on [03/07/2026]. See the Terms and Conditions (https://onlinelibrary.wiley.com/terms-and-conditions) on Wiley Online Library for rules of use; OA articles are governed by the applicable Creative Commons License

For the treatment of tau aggregates with ACI-16664, the compound was dissolved in anhydrous dimethyl sulfoxide (DMSO, Sigma-Aldrich) at a concentration of 2.5 mM. In a black 384-well assay plate (Perkin-Elmer), 2N4R tau aggregates were diluted in PBS to 60 nM for heparin-seeded 2N4R tau aggregates or 250 nM for PHF-seeded 2N4R aggregates. To assess the selectivity of ACI-16664, heparin-induced 2N4R tau aggregates or Aβ1-42 aggregates were prepared as described above and diluted to 1 µM in PBS. Aggregates were then combined in technical duplicate with serial dilutions of compound at final concentrations ranging from 20 to 0.0048 µM, resulting in a final DMSO concentration of 4% and a total volume of 40 µL per well. The mixture was incubated for 30 min at RT, then 10 µL of 5 µM ThT in 250 mM glycine (both from Sigma-Aldrich) in PBS were added. Fluorescence (relative fluorescence units [RFU]) was measured on a TECAN SPARK multimode microplate reader (excitation: 448 nm; emission: 485 nm; with automatic detection of optimal gain). Compound activity, expressed as ThT RFU percentage reduction, was calculated and the half maximal inhibitory concentration (IC_{50}) was determined using GraphPad Prism (version 9.4 or higher, GraphPad Software) assuming an "[agonist] versus response–variable slope (four parameters)" model.

To assess compound activity when added at the start of an aggregation reaction, a first aggregation reaction was performed to generate large amounts of seeds, and 35 µM of monomeric 2N4R were mixed with human PHF diluted at 1:800 in PBS in a total volume of 200 µL. The aggregation mix was incubated at 37°C for 72 h with shaking at 1000 rpm. Aggregation of the tau protein was confirmed at the conclusion of the 72-h incubation time using the ThT assay. These aggregates were then used as seeds for the kinetic ThT assay to assess the inhibition of tau aggregation. In a 96-well plate (Greiner, Catalog No.:655096), the following aggregation mix was prepared in PBS: 4 µM monomeric 2N4R tau, 0.35 µM PHF seeded tau 2N4R aggregates, DTT 10 mM, ThT 1 µM, ACI-16664 25 µM, or 1% DMSO. Control reactions contained the same reaction mix but no tau monomer or no PHF-seeded tau 2N4R aggregates. The 96-well plate was sealed and incubated for 24 h at 37°C with constant agitation at 270 rpm inside the Tecan Spark multimode microplate reader (excitation: 448 nm; emission: 485 nm; read every 30 min, fixed manual gain).

2.5 | Recombinant α-synuclein seeds

Full-length α-synuclein (αSyn) (R Peptide, Catalog No.: S-1153-4) was prepared in 50 mM Tris–HCl, 115 mM NaCl, pH 7.4, at a protein concentration of 1 mg/mL. Samples were incubated for 7 days at 37°C under orbital shaking at 1000 rpm. Fibrils were collected by centrifugation at 20,000 × g for 1 h, and the pellets were resuspended in Dulbecco's phosphate-buffered saline (DPBS) (pH 7.4) and sonicated (Sonic Dismembrator: 60 pulses at 30% power, 1.0 s ON/1.0 s OFF), aliquoted, snap-frozen in liquid nitrogen, and stored at −80°C as single-use aliquots.

2.6 | Multiple system atrophy (MSA)-amplified fibrils

Frozen brain tissue from multiple brain regions of a MSA donor (obtained from BioIVT) were processed at 10% (w/v) in DPBS containing complete protease inhibitor. Samples were homogenized on ice (IKA T10; setting 2-3), then sonicated on ice (Fisherbrand Model 120 Sonic Dismembrator, 50% amplitude, 1 s ON/1 s OFF, total 1 min) before clarification (3000 × g, 5 min, 4°C). The clarified homogenate was adjusted to 1% (v/v) Triton X100, mixed, and ultracentrifuged (100,000 × g, 30 min, 4°C). Pellets were washed in 1% Triton X100 in PBS, sonicated (50% amplitude, 0.5-s pulses, 30 cycles), and pelleted (100,000 × g, 30 min, 4°C). Detergent was removed with three DPBS washes; the final pellet was resuspended in DPBS and sonicated (50% amplitude, 0.5-s pulses, 30 cycles). The IF was aliquoted for single use and stored at −80°C.

Fibril amplification was achieved by two sequential passages in primary rat neuronal cultures. In Generation 1 (G1), cultures at Day In Vitro (DIV) 6 were exposed to IF seeds; in Generation 2 (G2), cultures at DIV6 were exposed to G1derived seeds. Before being added to cultures, seeds (IF or G1) were thawed and sonicated, then added to the neurons in Neurobasal++/B27 to a final 1.5% (v/v). Cultures were maintained at 37°C, 5% CO_2 until DIV25 to allow seeded aggregation of endogenous αSyn.

At DIV25, cultures were washed in DPBS and lysed on ice in buffer containing 50 mM Tris, 150 mM NaCl (pH 7.5), 1% Triton X100, protease inhibitors, phosphatase inhibitor cocktails 2 and 3, and 3 mM PMSF. Lysates were sonicated on ice (Fisherbrand Model 120, 50% amplitude, 1 s ON/1 s OFF, 60 cycles) and ultracentrifuged (100,000 × g, 60 min, 4°C). Pellets were washed twice with ice-cold DPBS, resuspended in ice-cold PBS, and sonicated again on ice (50% amplitude, 1 s ON/1 s OFF, 120 cycles), aliquoted, flashfrozen, and stored at −80°C as single-use lots. The G2 material was produced identically, with G1 serving as the seeding input in place of IF. The G2 material is used as MSA-amplified material to trigger αSyn aggregation in the primary neuronal seeding assay.

2.7 | Attenuated Total Reflection Infrared spectroscopy (ATR-IR)

30 µM PHF-seeded recombinant 2N4R tau aggregates were prepared as described above. For treatment with ACI-16664, the compound was dissolved in DMSO (Sigma-Aldrich) at a concentration of 100 µM, resulting in a final DMSO concentration of 4%. The mixture was then incubated for 24 h at 37°C with shaking at 1000 rpm. All ATR-IR measurements were performed using a Tensor 27 spectrometer (Bruker) equipped with a BioATR II micro ATR accessory (Confocheck) for sample detection and temperature control. Spectra were acquired in absorbance mode over the spectral range of 4000 to 900 cm^{-1} at a resolution of 2 cm^{-1}, with 2000 scans averaged for both sample

15525279, 2026, 7, Downloaded from https://alz-journals.onlinelibrary.wiley.com/doi/10.1002/alz.71572 by Schweizerische Akademie Der, Wiley Online Library on [03/07/2026]. See the Terms and Conditions (https://onlinelibrary.wiley.com/terms-and-conditions) on Wiley Online Library for rules of use; OA articles are governed by the applicable Creative Commons License

and background. The spectrometer was equipped with a KBr beam splitter, a mid-infrared (MIR) source, an open optical filter, and a 6-mm aperture. The scanner velocity was set to 20 kHz, and signal gain for both sample and background was set to automatic. Acquisition was performed in double-sided forward-backward mode using a Blackman-Harris 3-Term apodization function, a zero-filling factor of 4, and phase correction via the Mertz method. Interferogram non-linearity correction was applied prior to Fourier transformation. After background acquisition, 15 µL of sample was applied to the ATR crystal and gently dried under a nitrogen stream for approximately 15 min, until a dry film formed. The baseline stability of water absorption bands (3500 to 3000 cm^{-1} and 2300 to 2000 cm^{-1}) was monitored to confirm drying. Subsequently, 15 µL of deuterium oxide (D_2O) (Sigma Aldrich; 151882) was added to the film, followed by identical drying until the D_2O bands (2800 to 2000 cm^{-1}) disappeared or stabilized. A final addition of 15 µL D_2O was made, and spectra were recorded. Spectral data were processed using OPUS 8.8 (Bruker). Each spectrum was normalized using the "vector normalization" method, then truncated to the amide I region (1700 to 1600 cm^{-1}) using the "cut" function. Baseline correction was performed with an iteration value of 1 using the "baseline correction" method. Processed spectra were exported and analyzed in GraphPad Prism 10.

2.8 | Micro-radiobinding assay

AD tau PHF (prepared as described above followed by dilution 9× in PBS) or aggregated recombinant 2N4R tau (diluted to 200 nM in PBS) were spotted (36 nL/spot) by electric pulse on an APS-coated glass slide (Electron Microscope Science, Catalog No.: 63475-AP) using the GeSim micro spotter (GeSim mbH Germany). The glass slides were mounted with a slide chamber with 64 wells in order to create individual hermetic wells. The chambers were blocked with Tris 50 mM pH 7.4/1% bovine serum albumin for 1 h at RT to decrease non-specific binding. The blocking buffer was then replaced with tritiated ACI-16664 at concentrations ranging from 0.9 to 500 nM in a total volume of 40 µL Tris 50 mM pH 7.4/Tween 0.1%. This experiment was used to determine total binding activity, while a parallel experiment in the presence of an excess (3 µM) of unlabeled ACI-16664 was used to determine non-specific activity. The chambers were sealed to avoid evaporation and incubated for 2 h in a 25°C incubator. The slides were then washed five times with ice-cold washing buffer (50 mM Tris-HCl, pH7.5), once with double-distilled water, and finally were left to dry under a stream of argon. Once the slides were fully dried, they were exposed and scanned in a real-time autoradiography system (BeaQuant, ai4R) for 16 h. Following digital imaging, quantification of signal was performed using the image analysis software Beamage (ai4R). Specific binding was calculated by subtracting the non-specific signal from the total signal. Data were analyzed in GraphPad Prism by applying a non-linear regression curve fit using a one site-specific binding model to calculate K_d values.

2.9 | Rat cortical neuron (RCN) cultures

Primary cortical neuron cultures used in the seeding assay and in the toxicity assay with recombinant aggregates are cultures that are highly enriched in neurons (with a minority of astrocytes and no microglia), prepared from post-natal day 1 (P1) Sprague-Dawley rats (Charles River Laboratories, L'Arbresle, France), using a procedure adapted from Hirling et al.[29] Briefly, neocortex and hippocampus were isolated after removal of meninges, brainstem, olfactory bulbs, and subcortical regions. Tissue was minced and enzymatically dissociated in digestion medium containing 20 U/mL papain, 0.36% glucose, and 1 mg/mL L-cysteine for 30 min at 37°C. To terminate the enzymatic reaction, the supernatant was removed and replaced with digestion medium supplemented with 0.36% glucose and 1% trypsin inhibitor (Sigma, Catalog No.: T9253), followed by a 10-min incubation at 37°C. The suspension was centrifuged at 300 × g for 2 min at RT, and the supernatant was discarded. Cells were resuspended in trituration buffer (MEM supplemented with 0.36% glucose, 2 mM L-glutamine, penicillin/streptomycin, and 10% horse serum), mechanically dissociated by repeated trituration, and centrifuged again at 300 × g for 2 min. The resulting pellet was resuspended in adhesion medium (MEM, 0.36% glucose, 2 mM L-glutamine, penicillin/streptomycin, and 10% horse serum) and plated on poly-D-lysine-coated 96-well plates (Ibidi μ-Plate 96-well Square, Catalog No.: 89626) at a density of 60,000 cells/well in 200 µL/well. Cultures were incubated at 37°C in a humidified atmosphere containing 5% CO_2. Four hours after plating, the adhesion medium was replaced with growth medium consisting of phenol red-free Neurobasal Medium supplemented with 2 mM L-glutamine, B27 supplement (Gibco, Catalog No.: 17504-044), and penicillin/streptomycin. To inhibit glial proliferation, cytosine arabinoside (AraC) was added at 2.5 µM after 4 days in culture (DIV4). For the toxicity assay using AD brain-derived tau PHF, cortical cultures were prepared using a modified version of the protocol described above to increase the abundance of microglia and astrocytes. Specifically, AraC was added at DIV13 instead of DIV4. Additionally, at DIV8, half of the medium was removed and replaced with 50 µL of complete neurobasal medium complemented with N-Acetyl cysteine 5 µg/mL (Sigma, Catalog No.: A9165), Apo-transferrin 100 µg/mL (Sigma, Catalog No.: T2252), sodium selenite 100 µg/mL (Sigma, Catalog No.: S9133), insulin 100 ng/mL (Sigma, Catalog No.: I0516), rh TGF-Beta2 200 ng/mL (Peprotech, Catalog No.: 100-35B), rm IL-34 100 ng/mL (R&D, Catalog No.: 5195-ML-010/CF), and cholesterol 1.5 µg/mL (Avanti Polar, Catalog No.: 700000) to promote microglial growth. The presence of microglia and astrocytes was confirmed by immunocytochemistry using anti-Iba1 and anti-glial fibrillary acidic protein (GFAP) antibodies, respectively.

15525279, 2026, 7, Downloaded from https://alz-journals.onlinelibrary.wiley.com/doi/10.1002/alz.71572 by Schweizerische Akademie Der, Wiley Online Library on [03/07/2026]. See the Terms and Conditions (https://onlinelibrary.wiley.com/terms-and-conditions) on Wiley Online Library for rules of use; OA articles are governed by the applicable Creative Commons License

2.10 | Tau seeding in RCNs using human insoluble and soluble tau seeds

The RCN seeding assay was performed as previously described.[30, 31] Briefly, tau aggregation was seeded on DIV7 using AD brain-derived insoluble or soluble tau aggregates. Tau PHFs were used as insoluble tau seeds. The seeding assay experiments were repeated with three different pools of PHFs, each combining PHFs from six to seven AD donors. PHFs were added to the culture medium at dilutions between 1:500 and 1:4000, depending on the pool used. Soluble HMW tau aggregates, isolated from five AD patients by SEC as described above, were used as soluble tau seeds, diluted at 1:20 in the culture medium. Morphomers (or vehicle) were added simultaneously with the seeds. At DIV21, neurons were fixed and immunolabeled with the T49 antibody (1:1000; Sigma, Catalog No.: MABN827), which selectively detects rodent tau but not hTau and thus allowed for the visualization of de novo tau aggregation in rat neurons, without detecting the human seed. Additionally, cells were immunolabeled with a nuclear neuronal marker (NeuN antibody, 1:1000; Abcam, Catalog No.: ab177487) to quantify neuron numbers and a dendritic marker (Map2, 1:2000, Abcam, Catalog No.: ab5392) to assess neurite area. Cells were imaged using the InCell Analyzer 2200. Quantification of T49-positive tau aggregates (speckles) and NeuN-positive neuronal counts was performed using a custom ImageJ macro. Statistical analyses were conducted using GraphPad Prism version 10 (GraphPad Software, CA, USA). Dose–response curves for seeding inhibition by Morphomers were generated by fitting a four-parameter logistic (sigmoidal) model. Averaged dose–response curves were generated from multiple experimental repeats, and the absolute half-maximal inhibitory concentration (absolute IC_{50}) of the averaged curve was determined. This corresponds to the concentration of compound at which seeding levels are reduced by 50% compared to the vehicle (no compound) control.

2.11 | Neuronal toxicity assay

For the toxicity assay with recombinant PHF-seeded 2N4R hTau aggregates, neuronal cultures and aggregates were prepared as described above. Aggregates were diluted in culture medium to 1 or 1.6 µM tau monomer equivalents and incubated with either ACI-16664 or vehicle (0.2% DMSO) at 37°C for 4 h before the mix was added to neuronal cultures at DIV8. After 3 days of treatment (DIV11), cells were fixed and immunolabeled as described below. For the toxicity assay with AD brain-derived tau PHFs, a large pool of tau PHFs prepared from 18 individual AD donors was diluted 1:65 in culture medium, mixed with either vehicle (0.2% DMSO) or ACI-16664, and incubated at 37°C for 24 h before the mix was added to rat cortical cultures enriched in microglia and astrocytes (described above) at DIV8. The final concentration of AD brain-derived tau PHFs in the culture medium was 35 nM. Cells were fixed and immunolabeled after 13 days of treatment (DIV21). For both toxicity assays, cells were fixed at the indicated time points with 4% paraformaldehyde (PFA) for 15 min at RT and washed three times with PBS. Fixed cells were then blocked and permeabilized for 1 h at RT in 10% normal goat serum (NGS) and 0.25% Triton X-100 in PBS. Cells were then incubated overnight at 4°C with a chicken polyclonal anti-MAP2 antibody (1:4000; Abcam; Catalog No.: ab5392) in 5% NGS and 0.25% Triton X-100 in PBS. Cells were then washed three times with PBS and incubated with Alexa Fluor 647-conjugated goat anti-chicken secondary antibody (Invitrogen, Catalog No.: A32933), diluted 1:1000 in PBS, for 45 min at RT in the dark. Cells were then washed three times with PBS before imaging with an Incucyte Z S3 microscope at 20× magnification. Analysis of the neuritic network was then performed using the Neuro Track function of the Incucyte software. Neuronal health was assessed by quantifying neuritic network density, measured as neurite length per imaged area (mm/mm^2), using the NeuroTrack module of the Incucyte software. Tau-induced toxicity was calculated by comparing the neuritic density in cultures treated with tau aggregates (plus DMSO) to the average neuritic density of vehicle-only (DMSO) control cultures. Neuroprotection by ACI-16664 was quantified as the percentage reduction in the loss neuritic density relative to tau-only conditions.

2.12 | Alpha synuclein seeding in RCNs

Rat primary neurons plated at a density of 30,000/well in poly-D-lysine-coated 96-well plates and treated with Arabinose-C at DIV4 were further treated with αSyn recombinant seeds (prepared as described above) (final concentration 1 ng/mL) or MSA-amplified material (prepared as described above) (0.5% v/v) concomitantly to the test compounds at a range of doses (from 5 µM to 20 nM) or DMSO at DIV6. Cells were fixed in 4% formaldehyde at DIV15 (treatment with MSA-amplified material) or DIV18 (treatment with recombinant seeds) and washed three times with PBS. Fixed cells were then blocked and permeabilized for 1 h at RT in 10% NGS and 0.25% Triton X-100 in PBS. Cells were then incubated for 1 h at RT with a chicken polyclonal anti-MAP2 antibody (1:3000; Abcam; Catalog No.: ab5392) and an αSyn pS129 antibody (abcam, Catalog No.: ab51253, 1:500) in 5% NGS and 0.25% Triton X-100 in PBS. Cells were then washed three times with PBS and incubated with Alexa Fluor 647-conjugated goat anti-rabbit secondary antibody (Abcam, Catalog No.: A32733) and Alexa Fluor 488-conjugated goat anti-chicken secondary antibody (Abcam, Catalog No.: A11039), diluted 1:1000 in PBS, for 45 min at RT in the dark. Cells were then washed three times with PBS before imaging with the InCell Analyzer 2200. αSyn pS129 and MAP2 channels were segmented, and the total αSyn pS129- and MAP2-positive area per image was determined. The aggregate-to-cell ratio was defined as the aggregate area per MAP2 area (sum over each well):

$$\text{Ratio} = \frac{\text{Area aggregates}}{\text{Area neurons}}$$

The aggregate-to-cell ratio serves to determine the inhibition of de novo aggregate formation. The normalized inhibition was calculated

15525279, 2026, 7, Downloaded from https://alz-journals.onlinelibrary.wiley.com/doi/10.1002/alz.71572 by Schweizerische Akademie Der, Wiley Online Library on [03/07/2026]. See the Terms and Conditions (https://onlinelibrary.wiley.com/terms-and-conditions) on Wiley Online Library for rules of use; OA articles are governed by the applicable Creative Commons License

using the following formula:

$$\text{aSyn inclusion } (\%) = \frac{\text{Ratio}_{\text{compound}}}{\text{Ratio}_{\text{DMSO}}}$$

2.13 | Tg4510 study design

All mice used in this study were purchased from The Jackson Laboratory and housed at PsychoGenics, Inc. for the full duration of the in vivo study. All animal procedures were approved by the Institutional Animal Care and Use Committee (IACUC) of PsychoGenics, Inc. (OLAW Assurance No. D16-00732, A4471-01), which is accredited by AAALAC International. All procedures were conducted in accordance with the Animal Welfare Act and the Public Health Service Policy on Humane Care and Use of Laboratory Animals and complied with the *Guide for the Care and Use of Laboratory Animals* (National Research Council, 2011) and associated National Institutes of Health guidelines. All mice were generated by crossing male hemizygous for the Camk2a-tTA transgene in B6 background with females hemizygous for the tetO-MAPT*P301L transgene in Friend Virus B background. Tg4510 mice used in the study were female hemizygous for both the Camk2a-tTA and the tetO-MAPT*P301L transgene. Female mice were used because tau pathology progresses more rapidly in females, allowing efficacy assessment within a shorter study timeline.[32, 33] Littermate controls (referred to as "tTA" in the manuscript) were female hemizygous for Camk2a-tTA and non-carriers of the tetO-MAPT*P301L transgene. Mice received oral gavage twice daily (BID) for 29 consecutive days, starting at 5 months of age and ending at 6 months of age. Sample size was determined based on power calculations from previous studies as described in the Statistics section. Mice were randomly allocated into the following treatment groups: tTa mice treated with vehicle BID ($n = 11$); Tg4510 treated with vehicle BID ($n = 20$); Tg4510 treated with ACI-16664 100 mg/kg BID (200 mg/kg/day total) ($n = 21$). ACI-16664 was formulated in 0.5% sodium carboxymethyl cellulose (CMC-Na, viscosity 400 to 800 cps) and 0.5% Tween 80 in water, at a dose volume of 10 mL/kg.

2.14 | Tissue collection

For terminal sample collection, mice were deeply anesthetized with isoflurane and placed in a stereotaxic frame. Terminal plasma samples were obtained via cardiac puncture in a subset of animals at predetermined time points (see below). Transcardial perfusion was performed, using chilled PBS (20 mM, pH 7.4, at RT) to clear blood from the brain vasculature. Brains were immediately extracted following perfusion and hemisected for downstream analysis. To enable both biochemical and histological analyses from each animal, the left hemisphere was used for biochemical assays and the right hemisphere for IHC. Left hemispheres were dissected to isolate the neocortex, which was snap-frozen in dry ice. Right hemispheres were immersion-fixed for 3 h in freshly prepared 4% PFA in PBS. Fixed tissue was cryoprotected in 15% sucrose/PBS, embedded in Optimal Cutting Temperature (OCT) compound, and snap-frozen in dry ice-cooled isopentane. A portion of the midbrain was harvested to measure compound concentrations in the brain.

2.15 | Plasma collection

Plasma samples were collected to generate compound plasma exposure data that were used to inform the pharmacokinetic model. Trough plasma samples were collected weekly, 1 h prior to the morning dose, via submandibular vein puncture in a subset of animals from each group on dosing days 7, 14, and 21. On day 27, trough samples were collected from all animals. Terminal plasma samples were obtained on day 29 (the day of sacrifice) via cardiac puncture in a subset of animals at predetermined time points: 1 h before the morning dose (corresponding to 23 h after dose) and at 2, 4, and 8 h after dose. For plasma preparation, whole blood was collected into K_2EDTA tubes and centrifuged at 3000 × g for 15 min at 5°C using a refrigerated centrifuge. The plasma supernatant was carefully transferred to fresh tubes and stored at −80°C until bioanalysis.

2.16 | Analysis of compound concentrations in brain and plasma

Frozen brain samples were homogenized in nine volumes (weight:volume) of IS solution (50% acetonitrile in water solution containing internal standard, 100 ng/mL Verapamil). An aliquot of 25 µL sample (brain homogenate sample or plasma) was mixed with 10 µL of control mouse plasma and further incubated with 800 µL IS solution in 1.5 mL centrifuge tube. The mixture was mixed by vortexing (~3 min) and centrifuged at 12,500 rpm for 5 min at 4°C. The supernatant was transferred to a fresh tube, and 1 µL of supernatant from each sample was injected for concentration analysis. Concentrations of ACI-16664 in brain homogenates and in plasma were measured using a liquid chromatography tandem mass spectrometry (LC-MS/MS)-based method, with a Triple Quad 6500+ instrument. A calibration curve with eight non-zero calibration standards was applied for the method including the upper and lower limit of quantification (ULOQ and LLOQ). LLOQ was set at 10 ng/g in brain and 1 ng/mL in plasma. A set of quality control (QC) samples consisting of four analyte levels (3 ng/mL, 40 ng/mL, 800 ng/mL, and 2400 ng/mL) were applied for the method. Data obtained from the LC-MS/MS were analyzed using GraphPad Prism to derive total brain concentrations of ACI-16664. For the exposure analysis, the calculated total compound concentrations were transformed into unbound concentrations in nM using the following formula: $\text{Unbound nM} = \frac{C \times 1000}{\text{MW}} \times f_{u,\text{brain}}$, where C (ng/g) is the total compound concentration in brain, MW (g/mol) is the molecular weight of the compound (375.38), and $f_{u,\text{brain}}$ (unitless) is the fraction unbound in brain (0.0067).

15525279, 2026, 7, Downloaded from https://alz-journals.onlinelibrary.wiley.com/doi/10.1002/alz.71572 by Schweizerische Akademie Der, Wiley Online Library on [03/07/2026]. See the Terms and Conditions (https://onlinelibrary.wiley.com/terms-and-conditions) on Wiley Online Library for rules of use; OA articles are governed by the applicable Creative Commons License

2.17 | Pharmacokinetic model

Because brain concentration data were sparsely sampled, a pharmacokinetic model was developed to estimate key steady-state exposure metrics, including the average brain concentration (Caverage). Pharmacokinetic parameters were estimated using a non-linear mixed-effects (NLME) modeling approach. The brain exposure model for ACI-16664 was developed using a combination of current experimental data and historical pharmacokinetic data from wild-type mice. Data preparation, exploratory analysis, and model pre- and post-processing were conducted in RStudio (version 3.6.3) using the IQRtools package (version 1.9.0). Parameter estimation for the NLME models was performed in Monolix (version 2019R1).

2.18 | Preparation of total cortical homogenates (TCHs) and soluble fractions

For the preparation of TCHs, frozen neocortex was resuspended in nine volumes per weight of ice-cold homogenization buffer (25 mM Tris-HCl pH 7.4, 150 mM NaCl, 1 mM EDTA, 1 mM EGTA) supplemented with phosphatase and protease inhibitors (30 mM NaF, 0.2 mM Na_3VO_4, 1 nM okadaic acid, 1 mM PMSF, 5 mM $Na_4P_2O_7$, and Roche protease inhibitor cocktail Complete). Homogenization was performed using a VWR pellet mixer in microcentrifuge tubes. Homogenates were aliquoted and stored at −80°C until use. Soluble HMW tau aggregates were isolated from Tris-soluble cortex homogenates by SEC, following a protocol adapted from Takeda et al.[25] Briefly, 400 µL of TCH was thawed on ice, diluted 1:1 in PBS, centrifuged for 1 min at 2000 × g, and filtered through a 0.22-µm Millex-GV syringe filter (PVDF, 33 mm) to remove residual tissue. SEC was performed on the resulting supernatant to isolate soluble HMW tau aggregates.

2.19 | Quantification of hTau by AlphaLISA

Total and aggregated hTau levels were quantified in TCH and SEC fractions using AlphaLISA (PerkinElmer) with the following antibody pairs: For total tau, HT7-acceptor beads + Tau13-biotinylated (Tau13-BT) were used. For aggregated tau, HT7-acceptor beads + HT7-biotinylated (HT7-BT) were used. Tau13-BT (Santa Cruz Biotechnology) and HT7-BT (Thermo Fisher Scientific) were used according to the manufacturer's instructions. HT7-acceptor beads were generated by crosslinking the HT7 antibody (clone MN1000, Thermo Fisher Scientific) to PerkinElmer acceptor beads using $NaBH_3CN$ following the manufacturer's protocol. In 384-well white OptiPlates (PerkinElmer), 5 µL of diluted sample was combined with 20 µL of the appropriate antibody mix: Tau13-BT (0.065 nM) and HT7-acceptor beads (2.5 µg/mL) for quantification of total tau, or HT7-BT (0.15 nM) and HT7-acceptor beads (1.25 µg/mL) for quantification of aggregated tau. After 1 h incubation at RT, 25 µL of Streptavidin Donor beads (25 µg/mL, PerkinElmer) were added under light-protected conditions. Plates were incubated for 30 min at RT, and luminescence was measured using a Spark instrument (Tecan). Signal intensities were converted into protein concentrations expressed in arbitrary units (A.U.) using a standard curve generated with serial dilutions of tau PHF. A.U. values were log-transformed, fitted by non-linear regression, then back-transformed and corrected for dilution.

2.20 | Quantification of total hTau by Western blot

Pools of TCH were prepared per mouse group using an equivalent volume of TCH per mouse for all mice of the group. Those samples were prepared for the Jess automated Western blot system (Protein Simple, Catalog No.: 004-650) according to the manufacturer's instructions. Briefly, 5× Fluorescent Master Mix was prepared from a lyophilized stock by the addition of 20 µL 10× Sample Buffer and 20 µL 400 mM DTT. Lyophilized Biotinylated ladder was resuspended in 20 µL deionized water. One part of 5× Fluorescent Master Mix was combined with four parts of sample lysate prior to boiling for 5 min at 95°C.

The Jess Microplate was filled according to the manufacturer's instructions with the biotinylated ladder, denatured sample, primary and secondary antibodies (anti-mouse secondary NIR antibody,Biotechne, Catalog No.: 043-821), antibody dilution solution, and wash buffer. The plate and cartridge were inserted into the Jess device, and the run was started. Tau primary antibody HT7 (Invitrogen, Catalog No.: MN1000) was diluted 1/500 in antibody diluent.

2.21 | Immunohistochemistry

Sagittal sections of brain hemispheres (10 µm thickness) were obtained using a calibrated Leica CM1950 cryotome. Sectioning started at a randomized position approximately 0.24 mm lateral to the midline. At each level, five consecutive sections were collected, followed by the exclusion of the subsequent 25 sections. This sampling protocol was repeated until 12 levels were acquired from the frontal cortex. Systematic random sets from seven sections per mouse (levels 2, 4, 5, 6, 7, 9, and 11) were selected for IHC. Sections were labeled with pan-neuronal marker (PNM), a cocktail of neuron-specific antibodies labeling soma, dendrites, and axons, Millipore, Catalog No.: MAB2300; 1:300), T22 (Sigma, Catalog No.: ABN454, 1:1000), Synaptophysin 1 (Synaptic Systems, Catalog No.: 101011; 1:500), and PSD95 (Synaptic Systems, Catalog No.: 124008; 1:500) or with ThioS (Sigma-Aldrich, Catalog No.: T1892; 0.5% in water) to visualize NFTs. All secondary antibodies were diluted 1:500: Donkey anti-Rabbit Alexa Fluor 555 (Invitrogen, Catalog No.: A-31572), Donkey anti-Mouse Alexa Fluor 647 (Abcam, Catalog No.: ab150107), Donkey anti-Mouse Alexa Fluor 555 (Abcam, Catalog No.: ab150106), and Donkey anti-Rabbit Alexa Fluor 647 (Abcam, Catalog No.: ab150075). Each section was counterstained with DAPI. All antibodies were diluted in antibody diluent (Dako, S 302283-2), and sections were incubated overnight with primary antibodies. Non-specific binding to endogenous mouse IgG was blocked with M.O.M. serum (Vector Labs, Catalog No.: MKB 2213-1)

15525279, 2026, 7, Downloaded from https://alz-journals.onlinelibrary.wiley.com/doi/10.1002/alz.71572 by Schweizerische Akademie Der, Wiley Online Library on [03/07/2026]. See the Terms and Conditions (https://onlinelibrary.wiley.com/terms-and-conditions) on Wiley Online Library for rules of use; OA articles are governed by the applicable Creative Commons License

before primary incubation. After three washes in PBS (5 min each), sections were incubated for 1 h at RT with secondary antibodies, washed again, and stained with DAPI for 20 min. Sections were rinsed in ddH_2O (2× 5 min) and mounted with coverslips. Negative controls included wild-type brain sections and omission of primary antibody (OPNCs). Sections were imaged at 10× on a Zeiss AxioScan.Z1 microscope equipped with LED illumination and bandpass filter sets corresponding to each fluorophore. Images were captured with an ORCA Flash 4.0 B&W camera. The software used for image analysis was Image Pro Premier version 9 (Media Cybernetics). Additional images were also acquired on a Zeiss LSM 780 AxioObserver, objective Plan-Apochromat 63×/1.40 Oil DIC M27 for visual inspection and QC of the results at higher resolution. Delineation of the frontal cortex, for cortex size determination and for defining the regions of interest (ROIs) for staining quantifications, was based on the Allen Brain Atlas (http://atlas.brain-map.org) mouse sagittal sections. Adaptive thresholds were calculated using the following formula: threshold = mean signal[ROI] + factor × St.Dev. of mean signal [ROI]. To quantify NFTs, limited adaptive thresholds were used to segment objects with a size range between 70 and 400 μm^2 and 8-bit gray value (0 to 255) limit. The reported readout was immunoreactive surface area (IR area as a percentage of ROI size) expressed as a percentage of the frontal cortex area in square millimeters (mm^2). To ensure accurate and unbiased quantification in three dimensions, all cell counts were performed using DAPI-generated nuclear masks for 3D debiasing. Cells were counted only in case of overlap with a minimum 20 μm^2 large nucleus, in a penumbra of two to three pixels around the nucleus, and with fill holes and eight-pixel connect options for segmentation switched on (the latter assure that each cell is counted just once and not fragmented pieces of it). To quantify the number of T22-positive cells, the number of cells positive for both T22 and NeuN was divided by the total number of NeuN-positive cells. Neurite preservation was assessed by delineating neurites based on PNM labeling and distinguishing them from soma using a computer learned algorithm taking into account the criteria of shape, size, and proximity to DAPI-stained nuclei. Synaptic integrity was assessed based on PSD95 or Synaptophysin1 labeling, segmenting images using adaptive thresholding, with size and intensity filters applied to exclude objects smaller than 1 μm^2 or below a minimum 8-bit grayscale intensity (0 to 255). Absolute immunoreactive area was then determined, corrected for artifacts such as missing tissue or folds. As an additional measure of synapse preservation, the number of Synaptophysin1-positive and PSD95-positive structures was quantified. Images were segmented after applying a Top Hat filter (two passes; strength 30 for PSD95 and 40 for Synaptophysin1) to optimize the detection of individual punctate structures. To quantify the size of the frontal cortex, systematic random sets from seven sections per mouse (levels 2, 4, 5, 6, 7, 9, and 11) were selected, and the region was manually delineated on brain sections. Brain ROIs of the frontal cortex sizes were determined using delineation based on the Allen Brain Atlas (http://atlas.brain-map.org) mouse sagittal section. Average surface area of the frontal cortex was then calculated and is expressed in mm^2.

2.22 | Statistics

All experiments were performed and analyzed blind to experimental groups. For in vitro experiments, means ± standard deviation (SD) are reported except when indicated and statistical significance was assessed based on one-way ANOVA. Sample size was determined based on power calculations derived from observed compound effects and readout variability in prior treatment studies using similar compounds. These analyses indicated that at least 18 mice per group were required to detect a 39% reduction in aggregated tau levels measured by the AlphaLISA assay using the HT7/HT7 tau antibody pair ($\alpha = 0.05$, 80% power). No outlier analysis was performed to exclude data. Statistical analyses of animal group means and differences in means were performed using linear mixed models, a class of models that takes into account both fixed and random factors. To account for animals not being single-housed, a random factor representing within-cage variability (or correlation) was included in the model. Independently of the response variable, the models contained the following factors: treatment (vehicle, ACI-16664 100 mg/kg BID) (fixed factor); cohort: 1 to 2, as categorical factor (fixed factor); cage (random factor). The response variable in each model was transformed, using the square root transformation to ensure adequate distribution and avoid heteroskedasticity. Linear mixed models were fitted using maximum likelihood and included an unstructured covariance. Degrees of freedom were approximated using the Satterthwaite's method. Pairwise group means differences of interest were assessed and corresponding uncorrected two-sided *p* values were reported. Pairwise least squares mean differences between groups and 95% confidence intervals (CIs) were reported and graphically displayed as forest plots on the back-transformed data scale. Furthermore, estimated pairwise least squares mean differences were reported as relative differences on the untransformed scale. In addition, data were represented graphically as dot plots per animal group, with mean and standard deviation, both on untransformed and transformed scale. No imputation was performed on missing data, and no rule for outlier definition was applied. All analyses were performed on the data available. Analyses were performed using the R statistical software (version 4.0.3), using mainly the following packages: lmer, emmeans, and ggplot2. Correlation between pairs of markers was assessed by treatment group and overall using pairwise complete observations. Spearman's rho correlation coefficient and associated *p* value against the hypothesis of absence of monotonic correlation were reported.

3 | RESULTS

3.1 | Identification of ACI-16664, a small molecule disrupting pathological tau β sheets

To identify compounds capable of disrupting pre-formed tau aggregates, small molecules from our proprietary Morphomer library were screened in vitro using heparin-induced aggregates of the longest

15525279, 2026, 7, Downloaded from https://alz-journals.onlinelibrary.wiley.com/doi/10.1002/alz.71572 by Schweizerische Akademie Der, Wiley Online Library on [03/07/2026]. See the Terms and Conditions (https://onlinelibrary.wiley.com/terms-and-conditions) on Wiley Online Library for rules of use; OA articles are governed by the applicable Creative Commons License

human tau isoform (hTau 2N4R). Aggregate integrity was assessed using the fluorescent dye ThT, which selectively binds β-sheet-rich structures, a hallmark of pathological tau aggregates that are absent in the monomeric, intrinsically unstructured physiological form.[34] Compounds that reduced ThT fluorescence after incubation with pre-formed hTau 2N4R aggregates were selected as initial hits. These hits were further optimized through an iterative and multiparameter medicinal chemistry strategy guided by structure activity relationships, yielding compounds with enhanced in vitro potency and improved physicochemical and pharmacokinetic properties, including solubility, permeability, and brain penetration.

These medicinal chemistry efforts led to the discovery of ACI-16664, a compound that reduced ThT fluorescence when incubated with pre-formed heparin-induced hTau 2N4R aggregates (Figure 1A; IC_{50} = 0.27 μM ± 0.04). A similar reduction was observed with pre-formed hTau 2N4R aggregates seeded by insoluble tau filaments from AD brains (AD tau PHFs; IC_{50} = 0.16 μM; Figure S1a) instead of heparin. Furthermore, when added at the onset of an aggregation reaction involving hTau 2N4R monomers and insoluble AD brain tau seeds (PHF), ACI-16664 completely prevented the appearance of ThT fluorescence (Figure 1B). These data indicate that ACI-16664 both disrupts pre-existing aggregates and also prevents the formation of new pathological tau β-sheet structures.

To evaluate the selectivity of ACI-16664 for tau aggregates relative to other amyloid proteins, ThT aggregation assays were performed using Aβ1-42 fibrils. Aβ fibrils treated with ACI-16664 showed only a minimal decrease in ThT signal, indicating >600-fold selectivity of the compound for tau over Aβ aggregates in this assay (Figure S1C). As a positive control for activity on Aβ, we also included a compound previously identified as an Aβ aggregation inhibitor, which produced the expected decrease in ThT signal (Figure S1D). These results indicate that the activity of ACI-16664 in the ThT assay is target-specific rather than reflecting a general effect on amyloid fibrils.

To further evaluate the impact of ACI-16664 on the structural integrity of tau aggregates, ATR-IR spectroscopy was employed as an orthogonal method to the ThT based assays. This method differentiates secondary protein structures based on distinct infrared absorption patterns.[35] Figure 1C show that PHF-seeded tau aggregates exhibited infrared absorption with maxima at wavenumbers 1624.1 ± 0.4 cm^{-1} and 1638 ± 0.3 cm^{-1}, that is, characteristic of β sheets. In contrast, tau monomers generated a different absorption profile with a maximum at 1645.2 cm^{-1} ± 2.2, that is, a value associated with disordered structures and consistent with the predominantly unstructured nature of monomeric tau.[36] Incubation of the pre-formed tau aggregates with ACI-16664 resulted in an intermediate infrared absorption profile (Figure 1C). Notably, the most pronounced loss of absorption after incubation with ACI-16664 occurred at β-sheet-associated wavenumbers, indicating a reduction in β-sheet content (Figure 1C,D). These findings confirm the ThT assay measurements performed on the same samples (Figure S1B). Collectively, the ATR-IR and ThT assay results demonstrate that ACI-16664 disrupts the pathological β-sheet-rich structures characteristic of tau aggregates.

3.2 | ACI-16664 binds specifically to pathological tau aggregates

To assess the specificity and affinity of ACI-16664 binding to pathological tau, radiobinding experiments were performed using the tritiated compound. 3H-ACI-16664 bound to heparin-induced hTau 2N4R aggregates with an apparent Kd of 48 ± 9 nM and had no detectable binding to hTau 2N4R monomers (Figure 1E), indicating specific binding to the aggregated pathological form of tau. To assess whether ACI-16664 also bound to tau species present in AD patients, the radiobinding experiment was repeated with AD tau PHF. The results indicate binding with high apparent affinity (apparent Kd of 73 ± 16 nM), while no specific binding was detected with an identically prepared insoluble fraction from a non-diseased brain sample (Figure 1F). The selectivity of the compound against other physiological proteins was further investigated using a broad panel of 135 safety-relevant off-target proteins, and no significant off-target interactions were detected (data not shown). Together, these data demonstrate the high apparent affinity and specificity of ACI-16664 binding to the pathological, aggregated form of tau, with a selectivity that minimizes the risk of interference with monomeric tau or other physiological pathways.

3.3 | ACI-16664 inhibits tau seeding and toxicity in cortical neuron cultures

To investigate the consequences of ACI-16664 binding to tau aggregates in a cellular context, inhibition of intracellular tau seeding was assessed in primary rat cortical neurons (RCNs). Neurons were seeded using AD tau PHF and the appearance of tau inclusions evaluated 2 weeks later using a rodent-specific tau antibody, which selectively detected newly formed aggregates resulting from the recruitment of endogenous rat tau monomers (Figure 2A). Intracellular tau inclusions were robustly induced in cells incubated with AD tau PHF in the absence of compound. Importantly, the low concentration of tau seeds used in this assay did not affect neuron count or neurite area (Figure S2A-C), indicating that tau-induced toxicity was not observed under these conditions and allowing the assay to specifically assess tau seeding. Treatment with ACI-16664 substantially reduced the number of tau inclusions in a dose-dependent manner (IC_{50} = 1.6 μM; Figure 2A,B and S2A) without altering neuron number or neurite area (Figure S2B,C), indicating that the compound exerts its anti-aggregation activity with no detectable toxicity.

We previously showed that ACI-16664 selectively targeted tau aggregates over Aβ in biochemical, cell-free assays (Figure S1C,D). To further evaluate the selectivity of ACI-16664 in a cellular context, we tested its activity in a neuronal seeding assay using another amyloid protein as a seed. Because Aβ does not reliably seed aggregation in wild-type rodent neurons,[37] αSyn seeds were used as alternative β-sheet-rich protein aggregates capable of templated intracellular seeding. Seeds generated either from recombinant αSyn or from brain tissue of patients with MSA both induced robust intracellular aggre-

15525279, 2026, 7, Downloaded from https://alz-journals.onlinelibrary.wiley.com/doi/10.1002/alz.71572 by Schweizerische Akademie Der, Wiley Online Library on [03/07/2026]. See the Terms and Conditions (https://onlinelibrary.wiley.com/terms-and-conditions) on Wiley Online Library for rules of use; OA articles are governed by the applicable Creative Commons License

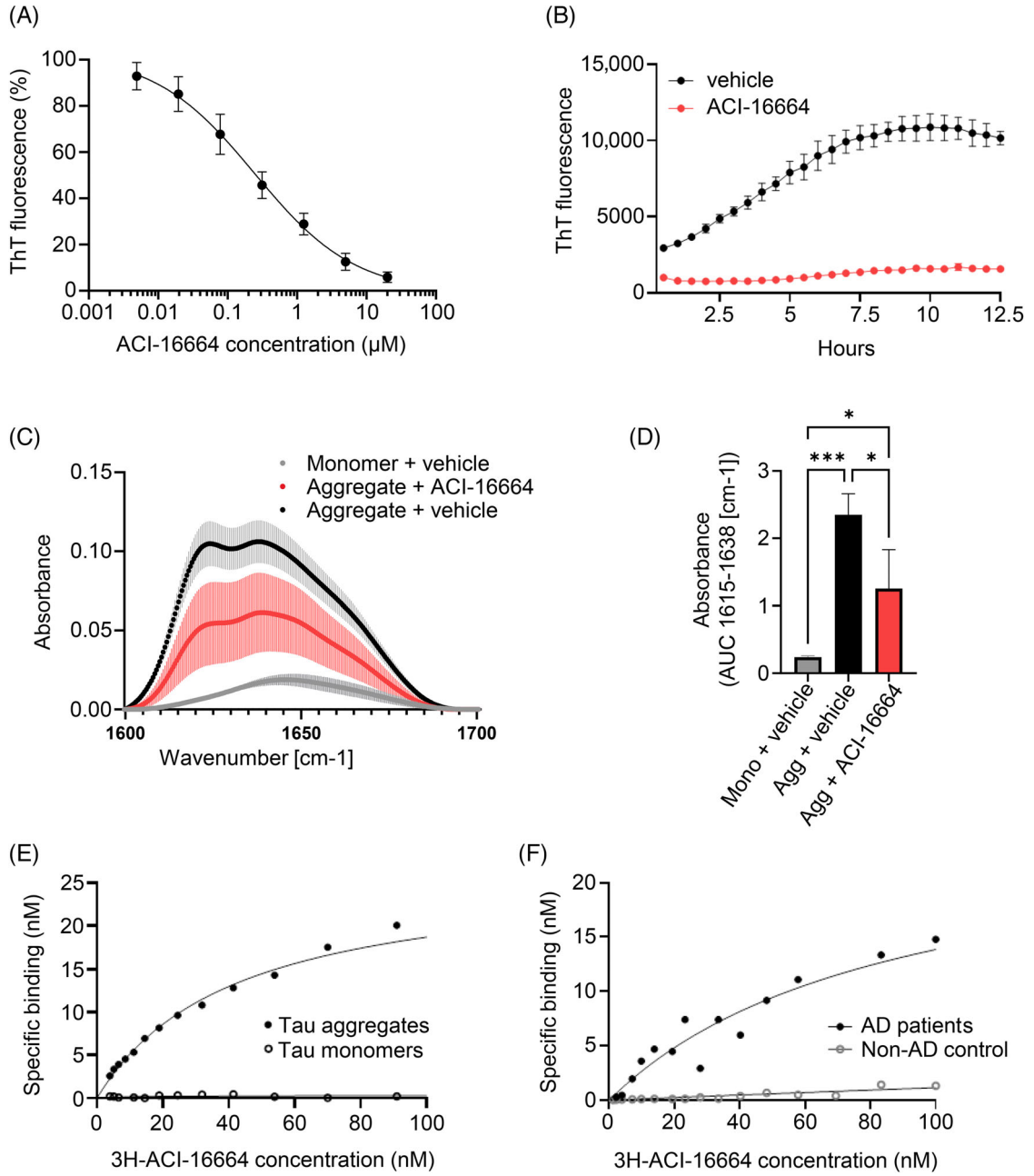

FIGURE 1 ACI-16664 specifically binds and disrupts aggregated tau. (A) ACI-16664 reduces the ThT fluorescence of hTau 2N4R aggregates (heparin-induced). hTau 2N4R aggregates were incubated with ACI-16664 for 30 min before ThT was added and fluorescence measured. ThT signal was normalized to the signal from aggregates that were not treated with compound. Data represent means ± SD of six independent experiments. (B) Treatment with ACI-16664 (25 uM) prevents increase in ThT fluorescence in an aggregation reaction initiated with hTau 2N4R monomers and PHF seeds. (C) Structural disruption of tau aggregates by ACI-16664 assessed by ATR-IR spectroscopy, focusing on the Amide I band (1600 to 1700 cm^{-1}), the region of the spectrum that is most sensitive to changes in protein conformation. PHF-seeded hTau 2N4R aggregates were incubated for 24 h at 37°C with vehicle (DMSO) or ACI-16664 (100 uM) before the samples were prepared for ATR-IR spectroscopy. Vehicle-treated hTau 2N4R monomers were also included to determine the ATR-IR profile of non-aggregated tau. Data represent means ± SD of four independent experiments. (D) Infrared absorbance measured between wavenumbers 1615 [cm^{-1}] and 1638 [cm^{-1}] of the absorbance spectra shown in (C), corresponding to the wavenumbers characteristic of beta sheets. Data represent the mean area under the curve (AUC, in cm^{-1}) ± SD of four independent experiments. Statistical significance * < 0.05; ** < 0.01; *** < 0.001 based on one-way ANOVA. (E) Affinity and specificity of 3H-ACI-16664 binding to recombinant tau aggregates were determined in a micro-radiobinding assay where increasing concentrations of tritiated compound were incubated with hTau 2N4R aggregates (heparin-induced) or with monomers. Data represent means ± SD of three independent experiments. (F) Apparent affinity and specificity of 3H-ACI-16664 binding to patient-derived pathological tau were determined in a micro-radiobinding assay where increasing concentrations of tritiated compound were incubated with tau PHF preparations from AD patients or with an equivalent preparation from a non-diseased control individual. The experiment was repeated using three different PHF preparations, each from a different donor. Data represent means ± SD of six independent experiments.

15525279, 2026, 7, Downloaded from https://alz-journals.onlinelibrary.wiley.com/doi/10.1002/alz.71572 by Schweizerische Akademie Der, Wiley Online Library on [03/07/2026]. See the Terms and Conditions (https://onlinelibrary.wiley.com/terms-and-conditions) on Wiley Online Library for rules of use; OA articles are governed by the applicable Creative Commons License

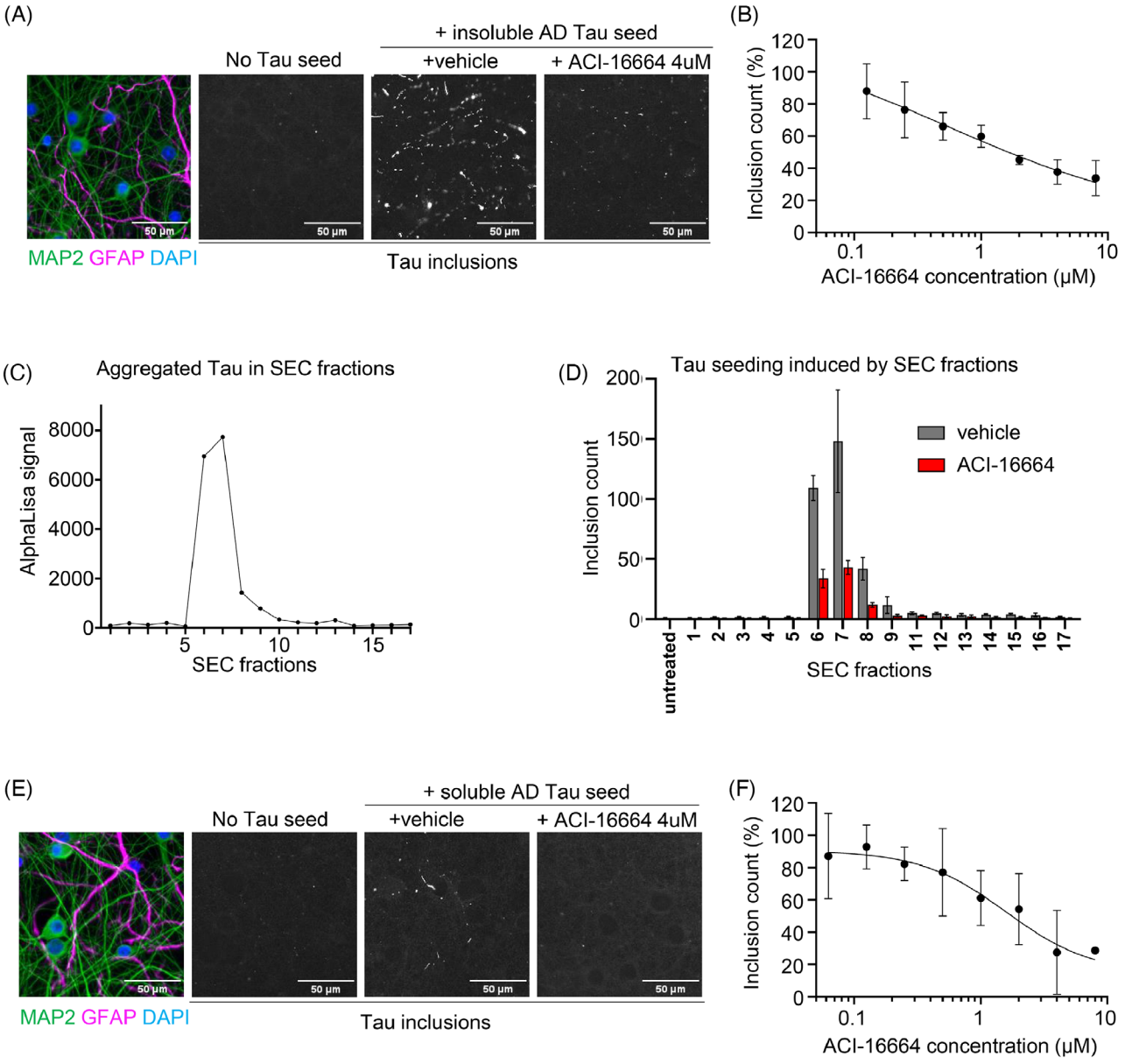

FIGURE 2 ACI-16664 inhibits the aggregation induced by insoluble and soluble AD brain tau seeds in rat cortical neurons. (A) ACI-16664 reduces tau inclusions induced by AD brain insoluble tau seeds (PHF) in rat cortical neuron cultures. Cells were treated with PHF from Day In Vitro (DIV) 7 to 21 in the presence or absence of ACI-16664 (4 uM) and were immuno-labeled with a rodent-specific tau antibody (T49) to monitor induced aggregation. The left panel shows a representative image of the culture used in this experiment, with nuclei stained with DAPI, astrocytes immunolabeled with anti-GFAP antibodies, and neurons immunolabeled with anti-MAP2 antibodies. (B) Quantification of the dose-dependent inhibitory effect of ACI-16664 on aggregation induced by AD brain insoluble tau seeds (PHF) in rat cortical neurons. The number of tau inclusions was normalized to the number of neurons and expressed as a percentage relative to controls treated with PHF and vehicle (no compound). Means ± SD of eight independent experiments are shown. (C) Identification of soluble HMW tau aggregate fractions from AD brains, prepared by fractionating soluble extracts using size exclusion chromatography (SEC) and collecting 1-mL fractions. Aggregated tau levels were quantified by AlphaLISA with the HT7/HT7 tau antibody pair, showing that most tau aggregates elute in HMW fractions 6 and 7. (D) ACI-16664 inhibits the seeding activity of AD brain-derived soluble HMW tau aggregate fractions in rat cortical neurons. Cultures were either untreated or treated with the indicated SEC fractions from pools of AD patients, in the presence of ACI-16664 4 µM or vehicle (DMSO) from DIV7 to DIV21, and tau inclusions were immunolabeled as described above. The total number of inclusions was counted in three culture wells, across 20 images per well. Bars represent the mean ± SD of the three culture wells without normalization. Corresponding neuron counts and individual well data are shown in Figure S3B,C. As an additional control, cultures were treated with soluble HMW fractions from non-AD controls, showing no induced aggregation (Figure S3B,C). (E) Representative images of rat cortical neurons treated as described in (D). The left panel shows a representative image of the culture used in this experiment, with nuclei stained with DAPI, astrocytes immunolabeled with anti-GFAP antibodies, and neurons immunolabeled with anti-MAP2 antibodies. (F) Quantification of the dose-dependent inhibitory effect of ACI-16664 on aggregation induced in rat cortical neurons by soluble HMW tau aggregate fractions 6 and 7 derived from AD brains (shown in panel C). The number of tau inclusions was normalized to the number of neurons and expressed as a percentage relative to controls treated with soluble HMW tau seeds and vehicle (no compound). Means ± SD of three independent experiments are shown.

15525279, 2026, 7, Downloaded from https://alz-journals.onlinelibrary.wiley.com/doi/10.1002/alz.71572 by Schweizerische Akademie Der, Wiley Online Library on [03/07/2026]. See the Terms and Conditions (https://onlinelibrary.wiley.com/terms-and-conditions) on Wiley Online Library for rules of use; OA articles are governed by the applicable Creative Commons License

gation in RCNs (Figure S2D,E). αSyn seeding was not inhibited by ACI-16664, in contrast to the compound's effect on tau seeding, further supporting the selectivity of ACI-16664 for tau aggregates over other amyloid proteins.

Given the biological relevance of soluble tau aggregates in tau seeding and spreading mechanisms, we next assessed whether ACI-16664 was also able to reduce the intracellular seeding induced by soluble HMW tau aggregates. For this, soluble proteins were isolated from AD brains, fractionated by SEC, and fractions rich in tau aggregates were identified using an AlphaLISA assay. As expected, tau aggregates were mostly found in the HMW fractions (Figure 2C; fractions 6 and 7, corresponding to sizes larger than the 669 KDa molecular weight marker; Figure S3A), consistent with previous findings.[25] When incubated with cortical neurons, these soluble HMW tau aggregates induced the formation of intracellular rodent tau inclusions (Figure 2D,E). Equivalent SEC fractions isolated from non-demented control individuals did not induce tau seeding (Figure S3B,C), consistent with the lack of tau pathology in these individuals.[25] When ACI-16664 was added with the soluble seeds to the neurons, induction of rat tau inclusions was significantly reduced (Figure 2D-F and S3B) with a potency (IC_{50} = 1.2 μM; Figure 2F) comparable to that observed with insoluble tau PHF seeds. Taken together, these data indicate that ACI-16664 prevents intracellular seeding induced by insoluble and soluble AD brain tau seeds.

To determine whether ACI-16664 mitigates pathological tau-induced toxicity, a cellular assay was established using RCNs where extensive neurite loss occurs within 3 days following the addition of tau aggregates (PHF-seeded hTau 2N4R; Figure 3A). Unlike the seeding assays presented above, which used patient-derived tau to assess the compound's effect on aggregation, this experiment used aggregates assembled from recombinant tau. Recombinant full-length tau aggregates showed no detectable seeding activity in RCNs (data not shown), consistent with previous work showing that efficient neuronal seeding requires post-translational modifications such as phosphorylation in the fuzzy coat region.[38] Nevertheless, extracellular recombinant or brain-derived tau aggregates can induce rapid neurotoxicity within minutes after exposure, indicating that tau aggregates can exert toxic effects independently of seeded aggregation.[39–41] This allowed us to use recombinant tau aggregates to assess tau-induced toxicity independently of seeding. Pre-incubation of these tau aggregates with ACI-16664 reduced neurite loss by up to 50% (Figure 3A,B; relative EC50 = 70 nM). These data support that ACI-16664 detoxifies tau aggregates in addition to its seeding inhibition activity.

To test whether ACI-16664 also protects against toxicity induced by patient-derived tau, AD tau PHF was used to disrupt the neuritic network in RCNs (Figure 3C,D). Pre-treatment of AD tau PHF with ACI-16664 improved neurite preservation, reducing neurite loss by 53% (p = 0.01, compared to neurons treated with AD tau PHF and vehicle), demonstrating that ACI-16664 effectively counteracts neurotoxicity. In contrast, treatment of RCNs with ACI-16664 in the absence of tau aggregates did not alter neurite length or neuronal number (Figure S2B,C). These results indicate that the protective effect of ACI-16664 results from activity on tau aggregates rather than a general trophic effect. Taken together, these results illustrate that ACI-16664 alleviates the pathological properties of a broad range of tau aggregate species, including patient-derived soluble and insoluble forms. Thus, ACI-16664 would be expected to attenuate in vivo tau pathology progression and tau-mediated neurodegeneration.

3.4 | Treatment with ACI-16664 significantly reduces tau pathology in the Tg4510 mouse model

To assess whether the anti-aggregation and neuroprotective effects of ACI-16664 observed in vitro translated into therapeutic benefits in vivo, the compound was tested in the Tg4510 mouse model of human tauopathy. Tg4510 mice overexpress hTau with the P301L mutation under the forebrain-specific CamKII promoter and show not only rapid tau aggregation but also fast and progressive neurodegeneration.[42,43] By 5 months of age, mice display substantial NFTs, neuronal loss, and brain atrophy, with pathology progressing rapidly within a few weeks. Non-diseased littermate controls, referred to as tTA mice, were included in the study. These mice are genetically identical to Tg4510 animals except for the absence of the hTau transgene.

At the age of 5 months, the Tg4510 mice were treated for 4 weeks with either vehicle or ACI-16664 (100 mg/kg) administered twice daily by oral gavage. The dose was selected based on pharmacokinetic data (not shown) indicating that this regimen would maintain the average brain exposure of ACI-16664 (unbound concentrations) above the IC_{50} observed in the in vitro neuroprotection assay (70 nM). Potency in the neuroprotection assay was selected as the target brain exposure, as prevention of neurodegeneration is the most clinically relevant activity. No adverse effects were observed during the treatment period, as indicated by stable body weight and the absence of mortality or clinical signs (Table S1).

To confirm adequate brain exposure of ACI-16664, brain concentrations were measured at three time points on the final day of the 4-week treatment period (Figure S4A). Based on these data, a pharmacokinetic model was used to estimate the 24-h average brain concentration (Figure S4B). To determine the more pharmacologically relevant unbound brain concentration, the unbound fraction in brain tissue (fu, brain) was experimentally determined, enabling calculation of the 24-h average unbound brain concentration, which was estimated at 149 nM (Figure S4C). This indicates that brain exposure was maintained within the targeted therapeutic range.

To confirm the overexpression of hTau in Tg4510 mice, hTau levels were assessed in cortical homogenates (Figures 4A and S5A). As expected, Tg4510 mice expressed high levels of hTau, while tTA control mice showed no detectable expression. Treatment with ACI-16664 did not alter hTau levels, consistent with its lack of interaction with monomeric tau (Figure 1F).

To assess the in vivo efficacy of ACI-16664 in reducing pathological tau, aggregated hTau species, ranging from dimers to fibrils, were quantified in the cortical homogenates using a mono-epitope AlphaLISA (Figure 4B). Vehicle-treated Tg4510 mice exhibited high levels of aggregated hTau. In contrast, Tg4510 mice treated with ACI-16664

15525279, 2026, 7, Downloaded from https://alz-journals.onlinelibrary.wiley.com/doi/10.1002/alz.71572 by Schweizerische Akademie Der, Wiley Online Library on [03/07/2026]. See the Terms and Conditions (https://onlinelibrary.wiley.com/terms-and-conditions) on Wiley Online Library for rules of use; OA articles are governed by the applicable Creative Commons License

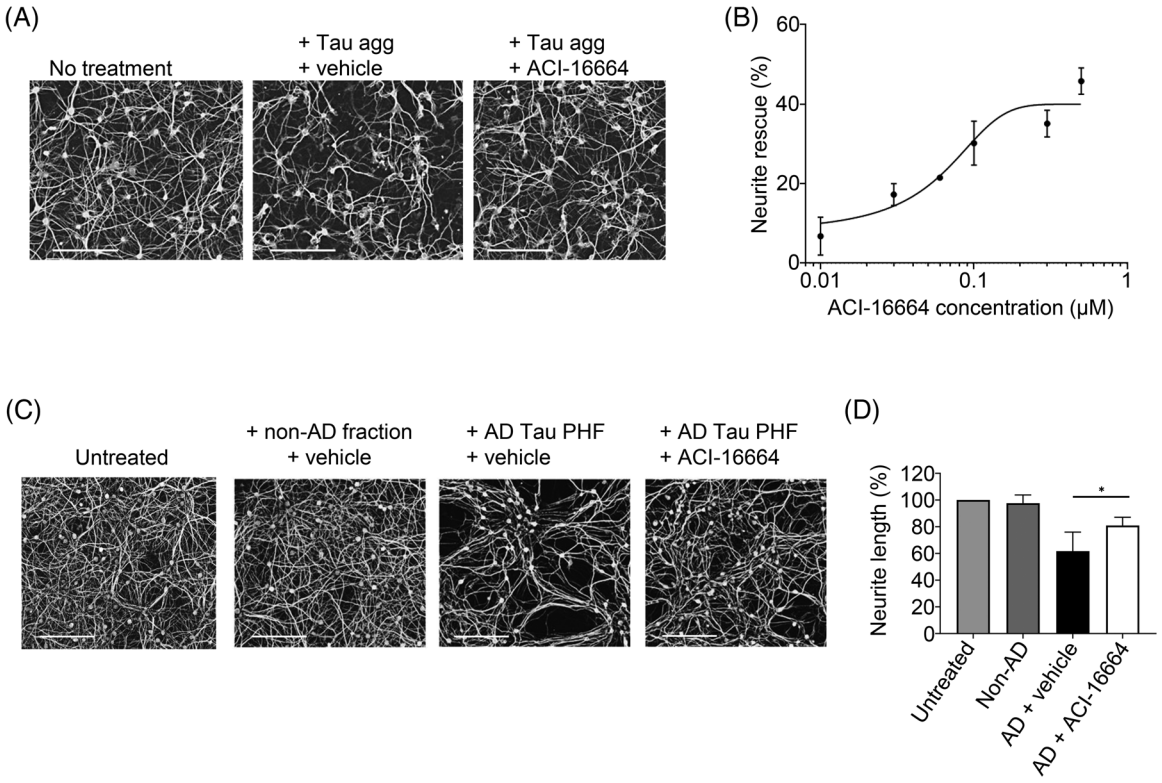

FIGURE 3 ACI-16664 reduces tau aggregate toxicity in rat cortical neuron cultures. (A) ACI-16664 reduces neurite loss in rat cortical neurons induced by PHF-seeded hTau 2N4R aggregates. Cells were either untreated or treated with pre-formed tau aggregates in the presence of ACI-16664 (250 nM) or vehicle (DMSO) from DIV 8 to DIV 11, and dendrites were then immunolabeled with anti-MAP2 antibodies. Scale bar: 200 μm. (B) Quantification of the dose-dependent rescue effect of ACI-16664 against the loss of neurites in rat cortical neurons. Total dendritic length per area (mm/mm^2) was assessed based on MAP2 immunolabeling, and neurite rescue was calculated as the percentage reduction in the difference between untreated cultures and cultures treated with tau aggregates in the absence of ACI-16664 (vehicle only). Means ± SEM of 6 independent experiments are shown. (C) ACI-16664 reduces neurite loss induced by AD brain tau PHF in rat cortical neuron cultures. Cells were untreated, treated with sarkosyl-insoluble fraction from non-AD controls ("non-AD fraction"), or treated with AD tau PHF in the presence of vehicle (DMSO) or ACI-16664 (250 nM) from DIV 7 to DIV 21 and dendrites were immunolabeled with anti-MAP2 antibodies. Scale bar: 200 μm. (D) Quantification of neurite length, expressed as a percentage of untreated controls, in cultures treated as described in (C). Means ± SEM of at least three independent experiments are shown. *P* values were calculated based on one-way ANOVA analysis.

showed a highly significant ($p < 0.001$) 51% reduction in aggregated hTau levels compared to vehicle-treated controls.

Given ACI-16664's inhibitory activity against both soluble and insoluble tau species in vitro, soluble aggregates and NFTs were evaluated in samples from the in vivo study. For soluble hTau aggregates in Tg4510 mice, Tris-soluble brain extracts were fractionated by SEC, and hTau was measured in each fraction (Figure 4C). This analysis was performed on pooled brain extracts from all mice within each treatment group to obtain sufficient material for SEC fractionation. hTau levels in the low-molecular weight (LMW) fractions remained largely unchanged following ACI-16664 treatment, as expected, as these mainly are composed of monomeric tau (Figure 4C,D). Strikingly, hTau levels in the HMW fractions were reduced by 52% in ACI-16664-treated mice compared to vehicle-treated controls. Quantification of aggregated hTau confirmed a 52% reduction in soluble HMW tau aggregates upon ACI-16664 treatment (Figure S5B,C). Reduced levels of soluble tau aggregates in ACI-16664-treated mice were also observed by IHC using the T22 antibody, which preferentially recognizes soluble tau oligomers.[44] As expected, vehicle-treated Tg4510 mice exhibited abundant T22 labeling in the frontal cortex, whereas no signal was detected in tTA controls (Figure 4E,F). ACI-16664 treatment led to a significant 31% reduction ($p = 0.008$) in T22-positive neurons compared to vehicle-treated mice. This reduction in T22 immunoreactivity, consistent with the reduction in soluble HMW tau measured by SEC fractionation, confirms that ACI-16664 reduces soluble tau aggregates in vivo.

To assess ACI-16664's effect on NFTs, ThioS was used as it preferentially labels mature NFTs, whereas less-fibril-rich pre-tangle structures typically do not produce detectable ThioS signal.[45,46] Moreover, to further ensure specificity, our analysis selectively quantified high-intensity ThioS-positive objects displaying tangle-like morphological characteristics as described in the Methods. NFTs were abundant in the frontal cortex of vehicle-treated Tg4510 mice and undetectable in tTA controls (Figure 4G,H). ACI-16664 treatment significantly reduced by 31% ($p = 0.001$) the cortical area covered by NFTs compared to vehicle-treated mice. To complement this analysis

15525279, 2026, 7, Downloaded from https://alz-journals.onlinelibrary.wiley.com/doi/10.1002/alz.71572 by Schweizerische Akademie Der, Wiley Online Library on [03/07/2026]. See the Terms and Conditions (https://onlinelibrary.wiley.com/terms-and-conditions) on Wiley Online Library for rules of use; OA articles are governed by the applicable Creative Commons License

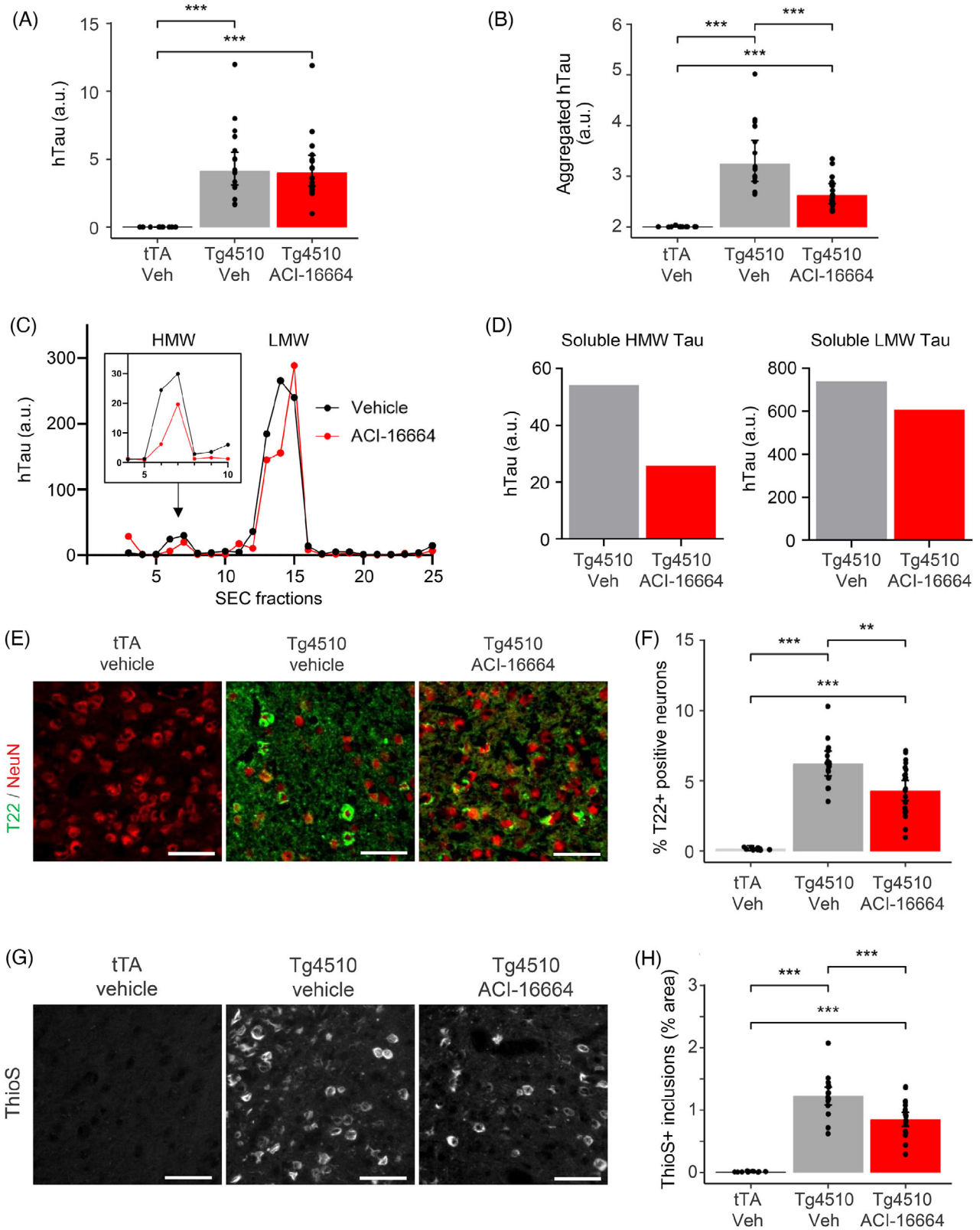

FIGURE 4 ACI-16664 treatment reduces soluble tau aggregates and tangles in the Tg4510 mouse model of tauopathy. (A) Similar hTau levels in ACI-16664-treated and vehicle-treated Tg4510 mice, measured in total cortex homogenates by AlphaLISA using the Tau13/HT7 tau antibody pair. No hTau was detected in tTA control mice. ACI-16664 (100 mg/kg) and vehicle were administered twice daily for a month, starting at 5 months of age. (B) Reduced levels of aggregated hTau in ACI-16664-treated compared to vehicle-treated mice, measured by AlphaLISA in total cortex homogenates using the HT7/HT7 tau antibody pair. (C) Reduced levels of soluble HMW tau aggregates in ACI-16664-treated, compared to vehicle-treated mice. Tris-soluble cortex extracts were fractionated by size exclusion chromatography (SEC), and hTau levels were assessed in each fraction by Tau13/HT7 AlphaLISA. HMW tau and low molecular weight (LMW) tau fractions are indicated. (D) hTau levels in HMW and LMW

15525279, 2026, 7, Downloaded from https://alz-journals.onlinelibrary.wiley.com/doi/10.1002/alz.71572 by Schweizerische Akademie Der, Wiley Online Library on [03/07/2026]. See the Terms and Conditions (https://onlinelibrary.wiley.com/terms-and-conditions) on Wiley Online Library for rules of use; OA articles are governed by the applicable Creative Commons License

with a classical histopathological marker of tau pathology progression, levels of phosphorylated tau (pS202/T205) were assessed using the AT8 antibody. AT8 immunoreactivity is widely used as a marker of tau pathology and correlates with disease progression in Tg4510 mice.[33] However, given the mechanism of action of ACI-16664, which targets tau aggregation, a reduction in AT8 signal would not necessarily be expected. Tau phosphorylation may precede aggregation or persist after aggregate disruption, such that a shift in the equilibrium from aggregated to non-aggregated tau may not directly translate into reduced AT8 immunoreactivity, particularly after a relatively short 1-month treatment. Consistent with this, AT8 immunoreactivity was also detected in the LMW tau SEC fraction of untreated Tg4510 mice (data not shown). Nevertheless, Tg4510 mice treated with ACI-16664 showed a 33% numerical reduction in AT8-positive neurons relative to vehicle-treated Tg4510 mice (Figure S5D,E), consistent with the reductions observed across the other tau pathology measures. This effect approached statistical significance ($p = 0.076$), which may reflect the more complex relationship between tau phosphorylation and aggregation, as well as the higher inter-animal variability of this readout. Collectively, the in vivo data indicate that ACI-16664 treatment significantly reduces both soluble pathological tau species as well as NFTs in Tg4510 mice, extending in vitro observations of activity against both soluble and insoluble AD tau seeds.

3.5 | ACI-16664 treatment significantly reduces tau-mediated neurodegeneration in Tg4510 mice

To assess whether the reduced tau pathology observed in ACI-16664-treated mice improved neuronal survival, neuronal loss in the frontal cortex was quantified following immunolabeling with NeuN, an antibody that labels the nuclei of neurons. Vehicle-treated Tg4510 mice exhibited a 24% neuronal loss in the frontal cortex compared to tTA control mice ($p < 0.001$; Figure 5A, with representative images shown in Figure S6A). Treatment with ACI-16664 significantly reduced this loss by half (48% reduction; $p = 0.002$; Figure 5A). Furthermore, the integrity of neuritic structures was assessed in the frontal cortex using the pan-neuronal marker (PNM), a monoclonal antibody (mAb) cocktail labeling axons, dendrites, and somas (Figure 5B and Figure S6B; see Materials and methods section for details on neurite delineation and quantification). Compared to tTA controls, neuritic structures were significantly reduced in vehicle-treated Tg4510 mice (by 29%, $p < 0.001$). Similar to the effect on neuronal cell count, treatment with ACI-16664 significantly improved neurite preservation, reducing neurite loss by 41% compared to vehicle-treated mice ($p = 0.005$).

Next, to evaluate whether treatment with ACI-16664 also prevented synapse loss, synapse integrity was assessed by immunolabeling pre- and post-synaptic structures using anti-synaptophysin 1 and anti-post-synaptic density protein 95 (PSD95) antibodies, respectively. In vehicle-treated Tg4510 mice, synaptophysin 1 and PSD95 immunoreactive areas were reduced by 28% and 39%, respectively, compared to tTA controls (Figure 5C,D and Figure S6C,D). Again, treatment with ACI-16664 also significantly preserved synaptophysin 1 and PSD95 reactive areas, reducing their loss by 25% ($p = 0.025$) and 21% ($p = 0.047$), respectively, compared to the vehicle treated mice. Similar results were obtained when counting synaptophysin 1- and PSD95-positive objects, with losses reduced by 21% ($p = 0.022$) and 27% ($p = 0.007$), respectively, confirming ACI-16664's protective effect on synaptic integrity. Together, these results show that in vivo treatment with ACI-16664 in Tg4510 mice preserved the integrity of neural network structures, including the most vulnerable to tau pathology, such as synapses, indicating improved neuronal health and survival.

Given the preservation of neurons, neurites and synapses, we next assessed whether these effects were translated into measurable brain tissue preservation at the macroscopic level. Cortical atrophy was evaluated by delineating and measuring the area of the frontal cortex. As shown in Figure 5E and Figure S6A, vehicle-treated Tg4510 mice exhibited a 31% reduction in cortical size compared to tTA controls, indicating significant neurodegeneration. In contrast, ACI-16664 treatment mitigated cortical atrophy, reducing tissue loss by 19% ($p = 0.031$ compared to the vehicle-treated mice), confirming an effect on overall brain tissue preservation.

To further investigate the relationship between different tau species and neurodegeneration in Tg4510 mice, we analyzed correlations of soluble tau and NFTs with multiple cellular endpoints (Figure 6). Most neuronal measures showed significant inverse correlations with both soluble tau aggregates and NFTs. Interestingly, however, some neuronal endpoints, such as the post-synaptic marker PSD95, correlated more strongly with soluble aggregates, while neuron counts as well as the pre-synaptic marker synaptophysin 1 and neurites were more closely associated with NFT levels. Cortical atrophy correlated to a similar extent with both soluble aggregates and NFTs, likely reflecting a cumulative impact on multiple structures, including neuronal somas, neurites, and synapses. These findings suggest that distinct neuronal structures are differentially affected by soluble versus insoluble tau species, with neuronal somas and pre-synaptic structures being more

fractions from (C) were quantified by summing signals from all fractions of each peak. (E) Representative images of frontal cortex sections immunolabeled for tau oligomers (T22 antibody) and neuronal nuclei (NeuN antibody), showing reduced levels of T22 signal in ACI-16664-treated compared to vehicle-treated mice. T22 staining was undetectable in tTA mice. Scale bar: 50 µm. (F) Quantification of the percentage of T22-positive neurons. (G) Representative images of frontal cortex sections stained with ThioS, showing reduced levels of neurofibrillary tangles in ACI-16664-treated Tg4510 mice. Staining was undetectable in tTA mice. Scale bar: 50 µm. (H) Quantification of percentage of frontal cortex area covered by ThioS-positive tangle-shaped inclusions. On the graphs of Figure 4A,B,F,H, individual values, group means, standard deviations, and uncorrected *p* values are shown. The statistical analyses were performed using the linear mixed-effects models predefined in the statistical plan of the study and described in the Methods. The study included 21 ACI-16664-treated Tg4510 mice, 20 vehicle-treated Tg4510 mice, and 11 vehicle-treated tTA mice.

15525279, 2026, 7, Downloaded from https://alz-journals.onlinelibrary.wiley.com/doi/10.1002/alz.71572 by Schweizerische Akademie Der, Wiley Online Library on [03/07/2026]. See the Terms and Conditions (https://onlinelibrary.wiley.com/terms-and-conditions) on Wiley Online Library for rules of use; OA articles are governed by the applicable Creative Commons License

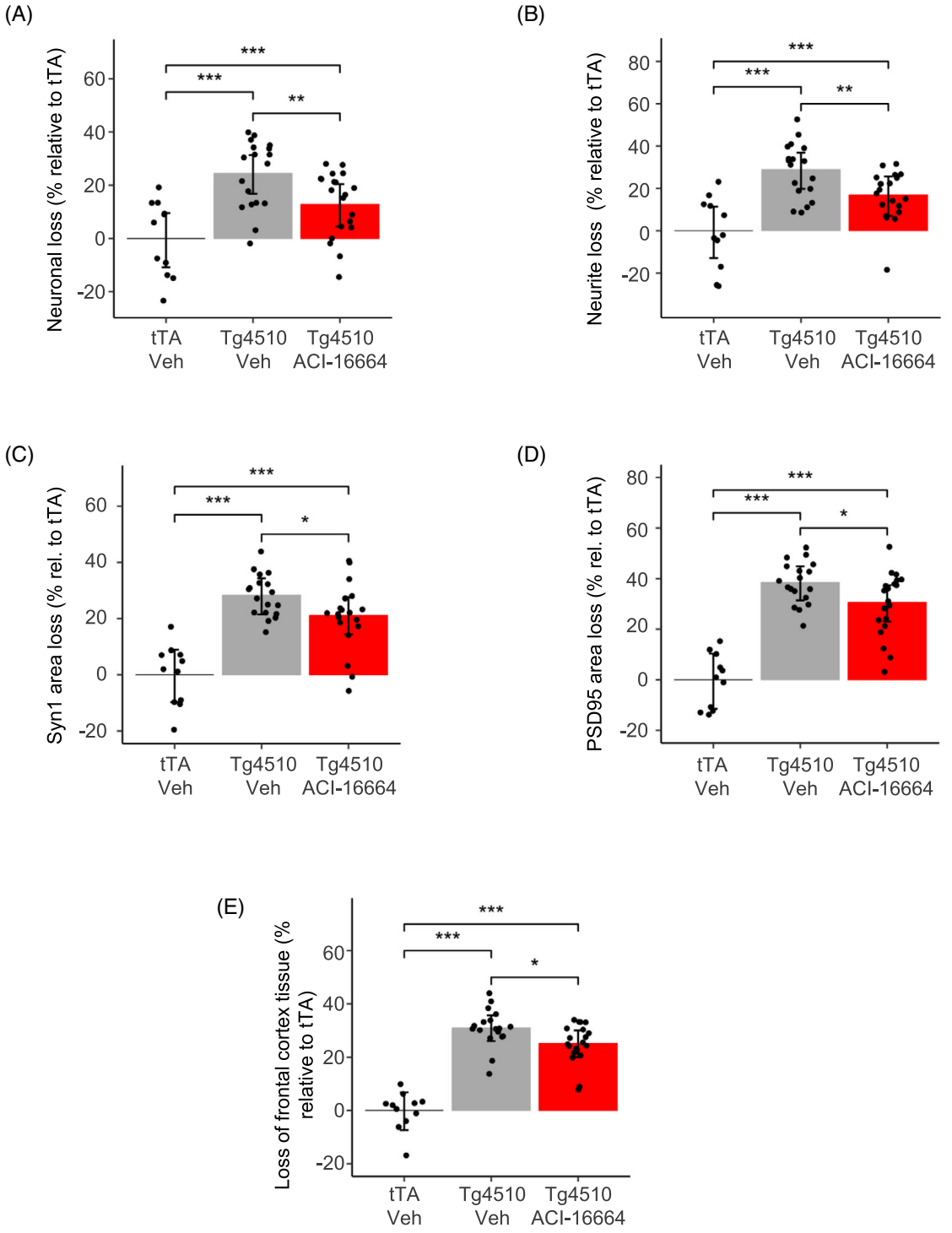

FIGURE 5 ACI-16664 treatment reduces neurodegeneration in Tg4510 mice. (A) Preservation of neuron number with ACI-16664 treatment. Neurons were counted in frontal cortex sections of 6-month-old Tg4510 mice based on NeuN immunolabeling. Neuronal loss was calculated by subtracting neuron counts in Tg4510 mice from the average count in tTA controls and expressed as a percentage of the tTA average. (B) Preservation of neurites with ACI-16664 treatment. Neurites were delineated and quantified in frontal cortex sections using immunolabeling with the pan-neuronal marker (PNM) antibody cocktail, as described in the Materials and methods section. Percentage loss was calculated as described in (A). (C) Preservation of pre-synaptic protein synaptophysin 1 (Syn1) levels with ACI-16664 treatment. Syn1-positive area was measured in frontal cortex sections, and percentage loss was calculated as described in (A). (D) Preservation of post-synaptic protein PSD95 levels with ACI-16664 treatment. PSD95-positive area was measured in frontal cortex sections, and percentage loss was calculated as described in (A). (E) Preservation of frontal cortex tissue size with ACI-16664 treatment. Frontal cortex size was measured as described in the Materials and methods section, and percentage loss was calculated as described in (A). For all panels in Figure 5, individual values, group means, standard deviations, and uncorrected *p* values are shown. The statistical analyses were performed using the linear mixed-effects models predefined in the statistical plan of the study and described in Methods.

15525279, 2026, 7, Downloaded from https://alz-journals.onlinelibrary.wiley.com/doi/10.1002/alz.71572 by Schweizerische Akademie Der, Wiley Online Library on [03/07/2026]. See the Terms and Conditions (https://onlinelibrary.wiley.com/terms-and-conditions) on Wiley Online Library for rules of use; OA articles are governed by the applicable Creative Commons License

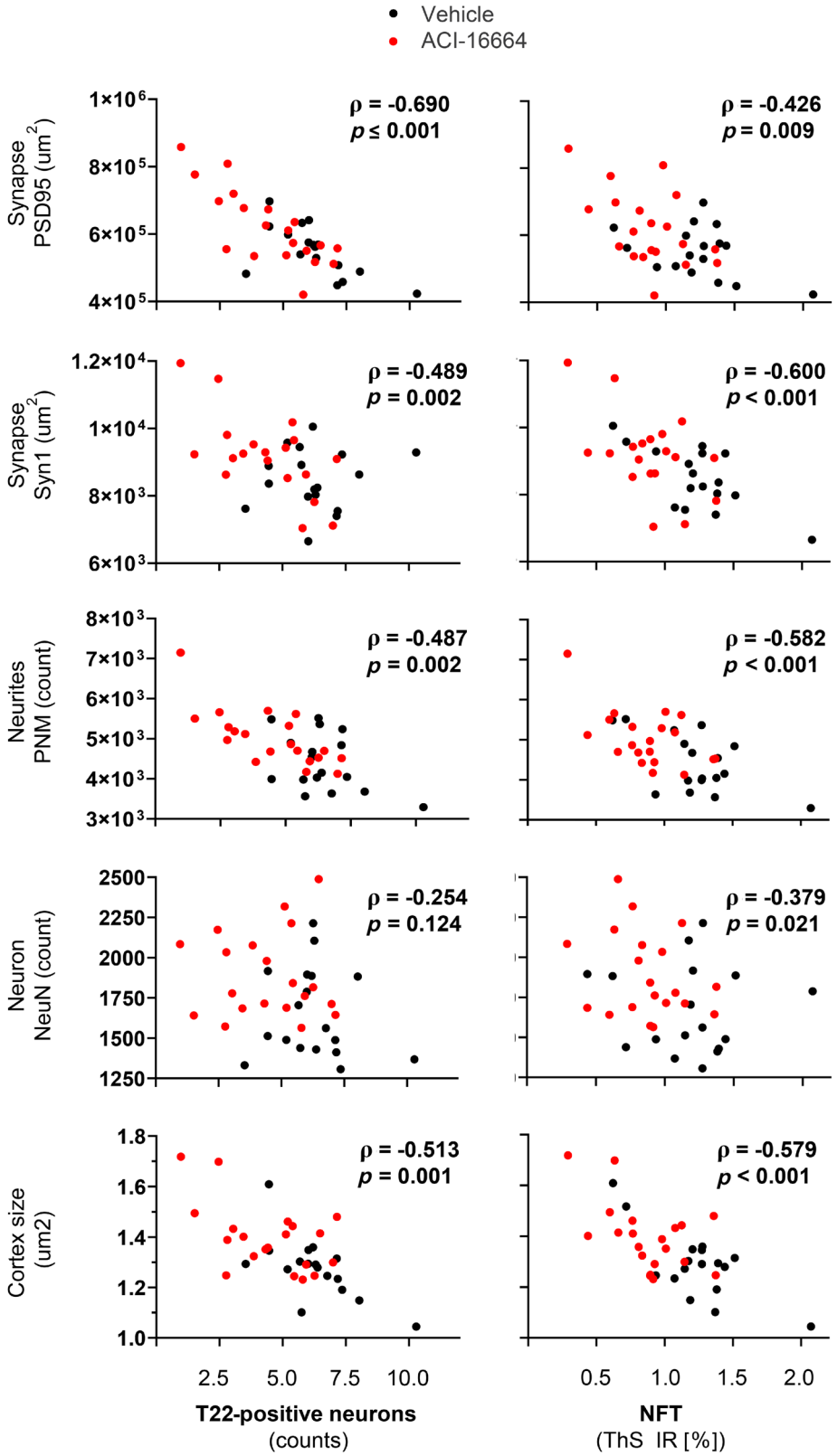

FIGURE 6 Brain preservation correlates with levels of soluble aggregates and tangles. Spearman correlations between tau pathology and brain preservation immunohistochemistry readouts (reported in Figure 4 and 5) in individual Tg4510 mice treated with vehicle or ACI-16664. Correlation coefficients (rho) and *p* values were calculated using combined data from both treatment groups.

15525279, 2026, 7, Downloaded from https://alz-journals.onlinelibrary.wiley.com/doi/10.1002/alz.71572 by Schweizerische Akademie Der, Wiley Online Library on [03/07/2026]. See the Terms and Conditions (https://onlinelibrary.wiley.com/terms-and-conditions) on Wiley Online Library for rules of use; OA articles are governed by the applicable Creative Commons License

vulnerable to NFTs and post-synaptic structures being more sensitive to soluble tau aggregates.

4 | DISCUSSION

Targeting pathological tau is considered one of the most promising approaches to treating or preventing AD and other tauopathies.[8,9] Yet developing drug candidates that specifically act on the diverse pathological forms of tau, both within brain cells and in the extracellular space, remains a challenge. Here, we describe ACI-16664, a brain and cell penetrant small molecule that is orally available and diffuses across cell membranes to engage pathological tau species in both compartments. In vitro, ACI-16664 structurally disrupts the β sheets of pre-formed tau aggregates, prevents tau seeding and aggregation induced by both soluble and insoluble AD-derived tau seeds, and reduces tau-induced neurotoxicity in rat primary neurons. In vivo, ACI-16664 reduces brain atrophy in the Tg4510 mouse model of tauopathy by significantly lowering levels of both soluble pathological tau aggregates and NFTs and preserving neuronal health.

Although the tau species driving neurotoxicity remain a matter of debate, the preservation of neurons, neurites, synapses, and cortex size in ACI-16664-treated Tg4510 mice demonstrates that this compound effectively targets toxic tau species in vivo. Our observations align with the growing body of evidence that soluble tau aggregates are key players in tau-mediated neurotoxicity.[20–23,47] ACI-16664 significantly reduced soluble tau aggregates, including T22-positive oligomers and soluble HMW tau aggregates. Interestingly, however, correlation analyses of data from ACI-16664- and vehicle-treated Tg4510 mice suggest that both soluble tau aggregates and NFTs contribute to neurodegeneration. The post-synaptic marker PSD95 correlated more strongly with soluble tau aggregates, whereas neuronal somas and pre-synaptic structures were more closely associated with NFTs. While the relative contribution of each tau species remains to be defined, our in vitro and in vivo data support the hypothesis that targeting both soluble and insoluble tau forms may offer the greatest therapeutic benefit in mitigating neurodegeneration in tauopathies.

The reduction in the levels and toxicity of pathological tau species upon treatment with ACI-16664 in Tg4510 mice may in principle result either from inhibition of de novo aggregation, leading to fewer newly formed toxic species, or from disruption of pre-existing tau aggregates, or both. Our in vitro studies support both mechanisms as ACI-16664 not only prevented the formation of new aggregates in cellular and cell-free assays but also acted on pre-formed aggregates, as shown by their structural disruption and a reduction in their associated toxicity in neurons. Notably, even in the presence of toxic but seeding-incompetent recombinant tau seeds, ACI-16664 reduced toxicity. This finding indicates that ACI-16664 can detoxify pathological tau through its action on pre-formed aggregates, independently of its ability to prevent further aggregation. This dual activity on both nascent and established aggregates may translate, in a clinical setting, into not only preventing disease progression but also mitigating tau pathology already established at the start of treatment. While the extent to which structural disruption by ACI-16664 leads to a reduction in pre-existing pathological tau burden remains to be determined, these findings raise the possibility of functionally reversing aspects of tau-mediated pathology.

Another notable feature of ACI-16664 is its selectivity for aggregated tau, with no detectable binding to the physiological monomeric form. This selectivity is key for minimizing the risk of side effects associated with disruption of normal tau function. Indeed, tau plays central roles in axonal transport, synaptic signaling and plasticity, mitochondrial regulation, and nuclear functions such as DNA protection and transcription.[1] Tau knockout mice display age-related motor and cognitive deficits,[48–51] while acute tau knockdown in adults impairs learning and memory.[52] Tau is also expressed in peripheral organs, with its loss affecting processes like glucose metabolism.[53,54]

Our data also provide insights into the biochemical mechanisms by which ACI-16664 exerts its anti-aggregation effects. Structurally, tau aggregates treated with ACI-16664 lose their ability to bind the β-sheet-specific dye ThT and display an altered ATR-IR spectroscopy profile indicating a loss of β-sheet structures. Under cell-free conditions, treatment of tau aggregates with ACI-16664 did not result in a measurable increase in soluble tau monomer (data not shown), indicating that the compound does not fully dissolve fibrils in this setting. Further studies will be required to determine the precise molecular fate of the remodeled fibrils and whether, in a cellular context, they are disassembled into monomers or cleared more efficiently. In vivo, a decrease in soluble tau aggregates (soluble HMW tau) was observed without a concomitant increase in the LMW tau fraction, which consists predominantly of monomeric tau. This pattern is consistent with a model in which ACI-16664 promotes the clearance of aggregated tau rather than simply shifting the equilibrium toward monomeric species. However, a shift toward monomeric tau cannot be excluded, as the LMW fraction is present in significant excess relative to HMW tau, and therefore the observed ~50% reduction in aggregates would be expected to produce only a modest relative increase in monomer levels. The remodeling of tau fibrils, whether or not it ultimately results in the clearance of pre-existing aggregates in a cellular context, likely also underlies the ability of ACI-16664 to prevent new aggregation. Since ACI-16664 does not interact with tau monomers, its inhibitory effect on aggregation must be initiated through binding to pre-existing aggregates. The disruption of tau β-sheet structures by ACI-16664 is expected to impair seeding and aggregate growth, as these structures are central to the templated aggregation mechanism underlying both processes. Similar anti-aggregation properties associated with β-sheet disruption have been described for epigallocatechin gallate (EGCG), a natural compound with poor brain penetration found in green tea.[55] Cryogenic electron microscopy studies revealed that interactions between EGCG and tau residues disrupted tau β-sheet structures by competing with tau–tau interactions and introducing a bend in the fibril, providing plausible mechanisms by which small molecules can destabilize tau aggregates.[56]

The limitations of this study include mainly those related to the Tg4510 mouse model, in which tau carries the P301L mutation found in some familial tauopathies but not in AD and folds differently within aggregates, resulting in fibrils that are structurally distinct from those

15525279, 2026, 7, Downloaded from https://alz-journals.onlinelibrary.wiley.com/doi/10.1002/alz.71572 by Schweizerische Akademie Der, Wiley Online Library on [03/07/2026]. See the Terms and Conditions (https://onlinelibrary.wiley.com/terms-and-conditions) on Wiley Online Library for rules of use; OA articles are governed by the applicable Creative Commons License

identified in human diseases. Nonetheless, ACI-16664 demonstrated potent in vitro activity against tau aggregates derived from AD brain tissue, including both soluble and insoluble species, indicating activity against a broad range of pathological tau species, including those relevant to human disease.

In summary, the data presented in our study show that the mode of action of ACI-16664 represents a unique and promising therapeutic approach for selectively targeting pathological tau, offering an unprecedented opportunity to counteract both pre-existing tau pathology and its progression in AD and other tauopathies.

AUTHOR CONTRIBUTIONS

MP, KF, LM, and PR contributed to the design, execution, analysis and interpretation of the in vitro cell-free experiments. KF, AL, PR, YV, and NAB contributed to the design, execution, analysis, and interpretation of the cellular assays. PR and KF designed, analyzed, and interpreted the biochemistry analyses of in vivo samples, which were conducted and analyzed by YV and KF. PR designed and supervised the in vivo study and interpreted the immunohistochemistry analyses. AF and KP made the predictions of the efficacious dose for the in vivo study and designed, supervised, analyzed, and interpreted the exposure measurements. NF performed all statistical analyses of the in vivo data. NP and FC contributed to the design and provided supervision of all aspects of the project. The overall project was initiated by PR, KF, NP, FC, VDa, VDe, SP, MKV, and AP. VDe, JM, SJ, and EG designed the small molecules. The first draft of the manuscript was written by NP, and all authors provided feedback on the manuscript.

ACKNOWLEDGMENT

Human brain samples were obtained from the following sources: (1) Tissue Solutions (now BioIVT); (2) the Netherlands Brain Bank: Netherlands Institute for Neuroscience, Amsterdam (open access: www.brainbank.nl); (3) the Banner Sun Health Research Institute Brain and Body Donation Program of Sun City, Arizona. The Brain and Body Donation Program has been supported by the National Institute of Neurological Disorders and Stroke (U24 NS072026 National Brain and Tissue Resource for Parkinson's Disease and Related Disorders), the National Institute on Aging (P30 AG019610 and P30AG072980, the Arizona Alzheimer's Disease Research Center), the Arizona Department of Health Services (contract 05700, Arizona Alzheimer's Disease Research Center), the Arizona Biomedical Research Commission (contracts 4001, 0011, 05-901 and 1001 to the Arizona Parkinson's Disease Consortium), and the Michael J. Fox Foundation for Parkinson's Research. We also thank our collaborators at Eli Lilly for their feedback at various stages of the project, including Suchira Bose for her technical advice on the RCN seeding assay. This work was funded by AC Immune.

CONFLICT OF INTEREST STATEMENT

All authors were employees or consultants at AC Immune SA during this work. Employees and consultants received salary or consulting fees from AC Immune SA. VDe, SJ, and EG are co-inventors on a patent related to this work. All authors except SP and LM received stocks or stock options from AC Immune SA. Author disclosures are available in the Supporting Information.

CONSENT STATEMENT

All human samples were collected from donors, for or from whom a written informed consent for a brain autopsy and the use of the material and clinical information for research purposes had been obtained.

REFERENCES

1. Kent SA, Spires-Jones TL, Durrant CS. The physiological roles of tau and Aβ: implications for Alzheimer's disease pathology and therapeutics. *Acta Neuropathol*. 2020;140(4):417-447. doi:10.1007/s00401-020-02196-w
2. Goedert M, Crowther RA, Scheres SHW, Spillantini MG. Tau and neurodegeneration. *Cytoskeleton (Hoboken)*. 2024;81(1):95-102. doi:10.1002/cm.21812
3. Creekmore BC, Watanabe R, Lee EB. Neurodegenerative disease tauopathies. *Annu Rev Pathol*. 2024;19:345-370. doi:10.1146/annurev-pathmechdis-051222-120750
4. Arriagada PV, Growdon JH, Hedley-Whyte ET, Hyman BT. Neurofibrillary tangles but not senile plaques parallel duration and severity of Alzheimer's disease. *Neurology*. 1992;42(3):631. doi:10.1212/WNL.42.3.631
5. Nelson PT, Alafuzoff I, Bigio EH, et al. Correlation of Alzheimer disease neuropathologic changes with cognitive status. *J Neuropathol Exp Neurol*. 2012;71(5):362-381. doi:10.1097/NEN.0b013e31825018f7
6. Cho H, Choi JY, Hwang MS, et al. In vivo cortical spreading pattern of tau and amyloid in the Alzheimer disease spectrum. *Ann Neurol*. 2016;80(2):247-258. doi:10.1002/ana.24711
7. Schöll M, Lockhart SN, Schonhaut DR, et al. PET imaging of Tau deposition in the aging human brain. *Neuron*. 2016;89(5):971-982. doi:10.1016/j.neuron.2016.01.028
8. Lane-Donovan C, Boxer AL. Disentangling tau: one protein, many therapeutic approaches. *Neurotherapeutics*. 2024;21(2):e00321. doi:10.1016/j.neurot.2024.e00321
9. Congdon EE, Ji C, Tetlow AM, Jiang Y, Sigurdsson EM. Tau-targeting therapies for Alzheimer disease: current status and future directions. *Nat Rev Neurol*. 2023;19(12):715-736. doi:10.1038/s41582-023-00883-2
10. Montine T, Phelps C, Beach T, et al. National Institute on Aging–Alzheimer's Association guidelines for the neuropathologic assessment of Alzheimer's disease: a practical approach. *Acta Neuropathol*. 2012;123(1):1-11. doi:10.1007/s00401-011-0910-3
11. Gómez-Isla T, Hollister R, West H, et al. Neuronal loss correlates with but exceeds neurofibrillary tangles in Alzheimer's disease. *Ann Neurol*. 1997;41(1):17-24. doi:10.1002/ana.410410106
12. Hyman B. All the Tau we cannot see. *Annu Rev Med*. 2023;74:503-514. doi:10.1146/annurev-med-042921-023749
13. Zwang TJ, del SastreE, Wolf N, et al. Neurofibrillary tangle-bearing neurons have reduced risk of cell death in mice with Alzheimer's pathology. *Cell Rep*. 2024;43(8):114574. doi:10.1016/j.celrep.2024.114574
14. Perez-Nievas BG, Stein TD, Tai H-C, et al. Dissecting phenotypic traits linked to human resilience to Alzheimer's pathology. *Brain*. 2013;136(Part 8):2510-2526. doi:10.1093/brain/awt171
15. Singh A, Allen D, Fracassi A, et al. Functional integrity of synapses in the central nervous system of cognitively intact individuals with high Alzheimer's disease neuropathology is associated with absence of synaptic Tau oligomers. *Journal of Alzheimer's Disease*. 2020;78(4):1661-1678. doi:10.3233/JAD-200716
16. Pichet Binette A, Franzmeier N, Spotorno N, et al. Amyloid-associated increases in soluble tau relate to tau aggregation rates and

15525279, 2026, 7, Downloaded from https://alz-journals.onlinelibrary.wiley.com/doi/10.1002/alz.71572 by Schweizerische Akademie Der, Wiley Online Library on [03/07/2026]. See the Terms and Conditions (https://onlinelibrary.wiley.com/terms-and-conditions) on Wiley Online Library for rules of use; OA articles are governed by the applicable Creative Commons License

cognitive decline in early Alzheimer's disease. *Nature Communications*. 2022;13(1):6635. doi:10.1038/s41467-022-34129-4

17. Dujardin S, Commins C, Lathuiliere A, et al. Tau molecular diversity contributes to clinical heterogeneity in Alzheimer's disease. *Nature Medicine*. 2020;26(8):1256-1263. doi:10.1038/s41591-020-0938-9
18. Glynn C, Rodriguez JA, Hyman BT. The structural line between prion and "prion-like": insights from prion protein and tau. *Curr Opin Neurobiol*. 2024;86:102857. doi:10.1016/j.conb.2024.102857
19. Mudher A, Colin M, Dujardin S, et al. What is the evidence that tau pathology spreads through prion-like propagation?. *Acta Neuropathol Commun*. 2017;5(1):99. doi:10.1186/s40478-017-0488-7
20. Taddei RN, Perbet R, Mate de Gerando A, et al. Tau oligomer–containing synapse elimination by microglia and astrocytes in Alzheimer disease. *JAMA Neurology*. 2023;80(11):1209-1221. doi:10.1001/jamaneurol.2023.3530
21. Lasagna-Reeves CA, Castillo-Carranza DL, Sengupta U, et al. Alzheimer brain-derived tau oligomers propagate pathology from endogenous tau. *Sci Rep*. 2012;2(1):700. doi:10.1038/srep00700
22. Ondrejcak T, Klyubin I, Hu N-W, et al. Tau and amyloid β protein in patient-derived aqueous brain extracts act concomitantly to disrupt long-term potentiation in vivo. *J Neurosci*. 2023;43(32):5870-5879. doi:10.1523/JNEUROSCI.0082-23.2023
23. Harris SS, Ellingford R, Hartmann J, et al. Alzheimer's disease patient-derived high-molecular-weight tau impairs bursting in hippocampal neurons. *Cell*. 2025;188(14):3775-3788.e21. doi:10.1016/j.cell.2025.04.006
24. Lasagna-Reeves CA, Castillo-Carranza DL, Sengupta U, et al. Alzheimer brain-derived Tau oligomers propagate pathology from endogenous Tau. *Sci Rep*. 2012;2:700.
25. Shuk Takeda, o, Susanne Wegmann, Hansang Cho, et al. Neuronal uptake and propagation of a rare phosphorylated high-molecular-weight tau derived from Alzheimer's disease brain. *Nature Communications*. 2015;6:8490. doi:10.1038/ncomms9490
26. Franzmeier N, Ewers M, Brendel M, et al. Earlier Alzheimer's disease onset is associated with a shift of tau pathology towards brain hubs which facilitates tau spreading. *Alzheimers Dement*. 2022;18(S6):e067043. doi:10.1002/alz.067043
27. Meisl G, Hidari E, Allinson K, et al. In vivo rate-determining steps of tau seed accumulation in Alzheimer's disease. *Sci Adv*. 2021;7(44):eabh1448. doi:10.1126/sciadv.abh1448
28. Rostagno A, Ghiso J. Isolation and biochemical characterization of amyloid plaques and paired helical filaments. *Curr Protoc Cell Biol*. 2009;44(1). doi:10.1002/0471143030.cb0333s44
29. Hirling H, Steiner P, Chaperon C, Marsault R, Regazzi R, Catsicas S. Syntaxin 13 is a developmentally regulated SNARE involved in neurite outgrowth and endosomal trafficking. *Eur J Neurosci*. 2000;12:1913-1923. doi:10.1046/j.1460-9568.2000.00076.x
30. Ficulle E, Kananathan S, Airey D, et al. A human tau seeded neuronal cell model recapitulates molecular responses associated with Alzheimer's disease. *Sci Rep*. 2022;12(1):2673. doi:10.1038/s41598-022-06411-4
31. Katsikoudi A, Ficulle E, Cavallini A, et al. Quantitative propagation of assembled human Tau from Alzheimer's disease brain in microfluidic neuronal cultures. *J Biol Chem*. 2020;295(37):13079-13093. doi:10.1074/jbc.RA120.013325
32. Yue M, Hanna A, Wilson J, Roder H, Janus C. Sex difference in pathology and memory decline in rTg4510 mouse model of tauopathy. *Neurobiol Aging*. 2011;32(4):590-603. doi:10.1016/j.neurobiolaging.2009.04.006
33. Song L, Lu SX, Ouyang X, et al. Analysis of tau post-translational modifications in rTg4510 mice, a model of tau pathology. *Mol Neurodegener*. 2015;10(1):14. doi:10.1186/s13024-015-0011-1
34. FitzpatrickAnthonyW P, Benjamin Falcon, Shaoda He, et al. Cryo-EM structures of tau filaments from Alzheimer's disease. *Nature*. 2017;547(7662):185-190. doi:10.1038/nature23002
35. Tatulian SA. Structural characterization of membrane proteins and peptides by FTIR and ATR-FTIR spectroscopy. *Methods Mol Biol*. 2013;974:177-218. doi:10.1007/978-1-62703-275-9_9
36. Mukrasch MD, Bibow S, Korukottu J, et al. Structural polymorphism of 441-residue tau at single residue resolution. *PLoS Biol*. 2009;7(2):E34. doi:10.1371/journal.pbio.1000034
37. Lacoursiere SG, Safar J, Westaway D, Mohajerani MH, Sutherland RJ. The effect of Aβ seeding is dependent on the presence of knock-in genes in the AppNL−G−F mice. *Front Dement*. 2022;1:941879. doi:10.3389/frdem.2022.941879
38. Kasen A, Lövestam S, Breton L, et al. Seed structure and phosphorylation in the fuzzy coat impact tau seeding competency. *Nat Commun*. 2025;16(1):9240. doi:10.1038/s41467-025-64312-2
39. Pareja-Navarro KA, King CD, Kauwe G, et al. Tau oligomers modulate synapse fate by eliciting progressive bipartite synapse dysregulation and synapse loss. *Mol Neurodegener*. 2026;21(1):13. doi:10.1186/s13024-026-00928-2
40. Harris SS, Ellingford R, Hartmann J, et al. Alzheimer's disease patient-derived high-molecular-weight tau impairs bursting in hippocampal neurons. *Cell*. 2025;188(14):3775-3788. doi:10.1016/j.cell.2025.04.006
41. Fá M, Puzzo D, Piacentini R, et al. Extracellular Tau oligomers produce an immediate impairment of LTP and memory. *Sci Rep*. 2016;6(1):19393. doi:10.1038/srep19393
42. Ramsden M, Kotilinek L, Forster C, et al. Age-dependent neurofibrillary tangle formation, neuron loss, and memory impairment in a mouse model of human tauopathy (P301L). *J Neurosci*. 2005;25(46):10637-10647. doi:10.1523/JNEUROSCI.3279-05.2005
43. SantaCruz K, Lewis J, Spires T, et al. Tau suppression in a neurodegenerative mouse model improves memory function. *Science*. 2005;309(5733):476-481. doi:10.1126/science.1113694
44. Lasagna-Reeves CA, Castillo-Carranza DL, Sengupta U, et al. Identification of oligomers at early stages of tau aggregation in Alzheimer's disease. *FASEB J*. 2012;26(5):1946-1959. doi:10.1096/fj.11-199851
45. Moloney CM, Lowe VJ, Murray ME. Visualization of neurofibrillary tangle maturity in Alzheimer's disease: a clinicopathologic perspective for biomarker research. *Alzheimers Dement*. 2021;17(9):1554-1574. doi:10.1002/alz.12321
46. Moloney CM, Labuzan SA, Crook JE, et al. Phosphorylated tau sites that are elevated in Alzheimer's disease fluid biomarkers are visualized in early neurofibrillary tangle maturity levels in the post mortem brain. *Alzheimers Dement*. 2023;19(3):1029-1040. doi:10.1002/alz.12749
47. Ondrejcak T, Klyubin I, Hu N-W, Rowan M. Patient brain-derived soluble tau rapidly and persistently disrupts synaptic plasticity in vivo. *IBRO Neurosci Rep*. 2023;15:S468. doi:10.1016/j.ibneur.2023.08.909
48. Ahmed VanderJeugd, et al. Cognition and hippocampal synaptic plasticity in mice with a homozygous tau deletion. *Neurobiol Aging*. 2014;35(11):2474-2478. doi:10.1016/j.neurobiolaging.2014.05.005
49. Ma Q-L, Zuo X, Yang F, et al. Loss of MAP function leads to hippocampal synapse loss and deficits in the morris water maze with aging. *J Neurosci*. 2014;34(21):7124-7136. doi:10.1523/JNEUROSCI.3439-13.2014
50. Regan P, Piers T, Yi J-H, et al. Tau phosphorylation at serine 396 residue is required for hippocampal LTD. *J Neurosci*. 2015;35(12):4804-4812. doi:10.1523/JNEUROSCI.2842-14.2015
51. Lei P, Ayton S, Moon S, et-al. Motor and cognitive deficits in aged tau knockout mice in two background strains. *Mol Neurodegener*. 2014;9:29. doi:10.1186/1750-1326-9-29
52. Velazquez R, Ferreira E, Tran A, et al. Acute tau knockdown in the hippocampus of adult mice causes learning and memory deficits. *Aging Cell*. 2018;17(4):e12775. doi:10.1111/acel.12775
53. Benderradji H, Kraiem S, Courty E, et al. Impaired glucose homeostasis in a Tau knock-in mouse model. *Front Mol Neurosci*. 2022;15:841892. doi:10.3389/fnmol.2022.841892

15525279, 2026, 7, Downloaded from https://alz-journals.onlinelibrary.wiley.com/doi/10.1002/alz.71572 by Schweizerische Akademie Der, Wiley Online Library on [03/07/2026]. See the Terms and Conditions (https://onlinelibrary.wiley.com/terms-and-conditions) on Wiley Online Library for rules of use; OA articles are governed by the applicable Creative Commons License

54. Wijesekara N, Gonçalves RA, Ahrens R, De Felice FG, Fraser PE. Tau ablation in mice leads to pancreatic β cell dysfunction and glucose intolerance. *FASEB J*. 2018;32(6):3166-3173. doi:10.1096/fj.201701352
55. Andreu-Fernández V, Almeida Toledano L, Pizarro N, et al. Bioavailability of epigallocatechin gallate administered with different nutritional strategies in healthy volunteers. *Antioxidants (Basel)*. 2020;9(5):440. doi:10.3390/antiox9050440
56. Seidler PM, Murray KA, Boyer DR, et al. Structure-based discovery of small molecules that disaggregate Alzheimer's disease tissue derived tau fibrils in vitro. *Nature Communications*. 2022;13(1):5451. doi:10.1038/s41467-022-32951-4

SUPPORTING INFORMATION

Additional supporting information can be found online in the Supporting Information section at the end of this article.

How to cite this article: Preitner N, Dehlinger V, Rodriguez P, et al. Elimination of tau tangles and soluble aggregates with the small molecule ACI-16664 prevents neurodegeneration in vivo. *Alzheimer's Dement*. 2026;22:e71572. https://doi.org/10.1002/alz.71572

15525279, 2026, 7, Downloaded from https://alz-journals.onlinelibrary.wiley.com/doi/10.1002/alz.71572 by Schweizerische Akademie Der, Wiley Online Library on [03/07/2026]. See the Terms and Conditions (https://onlinelibrary.wiley.com/terms-and-conditions) on Wiley Online Library for rules of use; OA articles are governed by the applicable Creative Commons License